Analyzing the Role of Air-Transportation in COVID-19 Pandemic Disaster

Final Report

APRIL 2023

SIRISH NAMILAE[1] and DAHAI LIU[2]

[1]Dept. of Aerospace Engineering, [2]College of Aviation

Embry-Riddle Aeronautical University, Daytona Beach, Florida 32114, USA

US DEPARTMENT OF TRANSPORTATION GRANT 69A3551747125

DISCLAIMER

The contents of this report reflect the views of the authors, who are responsible for the facts and the accuracy of the information presented herein. This document is disseminated under the sponsorship of the Department of Transportation, University Transportation Centers Program, in the interest of information exchange. The U.S. Government assumes no liability for the contents or use thereof.

1. Report No.	2. Government Accession No.	3. Recipient's Catalog No.
4. Title and Subtitle Analyzing the Role of Air-Transportation in COVID-19 Pandemic Disaster		5. Report Date APRIL 2023
		6. Source Organization Code
7. Author(s) SIRISH NAMILAE & DAHAI LIU		8. Source Organization Report No. CATM-2023-R2-ERAU
9. Performing Organization Name and Address Center for Advanced Transportation Mobility Transportation Institute 1601 E. Market Street Greensboro, NC 27411		10. Work Unit No. (TRAIS) 11. Contract or Grant No. 69A3551747125
12. Sponsoring Agency Name and Address University Transportation Centers Program (RDT-30) Office of the Secretary of Transportation–Research U.S. Department of Transportation 1200 New Jersey Avenue, SE Washington, DC 20590-0001		13. Type of Report and Period Covered Final Report: FEB 2019-JUNE 2020 14. Sponsoring Agency Code USDOT/OST-R/CATM
15. Supplementary Notes:		

16. Abstract

COVID-19 pandemic has resulted in an over 60% reduction in air travel worldwide according to some estimates. The high economic and public perception costs of potential superspreading during air travel necessitates research efforts that model, explain and mitigate disease spread. Here, we use a novel infection risk model that is linked with pedestrian dynamics to accurately capture these aspects of infection spread. The model is first parameterized through spatiotemporal analysis of a recent superspreading event in a restaurant in China. The passenger movement during boarding and deplaning, as well as the in-plane movement, are modeled with social force model and agent-based model respectively. We utilize the model to evaluate what-if scenarios on the relative effectiveness of policies and procedures such as masking and social distancing, as well as synergistic effects by combining different approaches in airplanes and other contexts. We then applied the dose response models to parametrically analyze the spread of infection and the effect of mask usage in generic transportation systems. We analyzed five empirical events of SARS-COV-2 transmission where the spatiotemporal details of the infected persons are known. We found that the dose level had a significant impact on the number of secondary infections. In general, mask usage reduced infections at all dose levels. High-quality N-95 masks are effective for all dose levels, while lower-quality masks exhibit a limited mitigation efficiency, especially for high-dose conditions. Sensitivity analysis indicated that the reduction in infection distance threshold is a critical factor in mask usage.

17. Key Words Point-process model, Secondary crash, Akaike Information Criterion (AIC)	18. Distribution Statement

19. Security Classif. (of this report) Unclassified	20. Security Classif. (of this page) Unclassified	21. No. of Pages 65	22. Price …

Form DOT F 1700.7 (8-72) Reproduction of completed page authorized

TABLE OF CONTENTS

EXECUTIVE SUMMARY

COVID-19 pandemic has resulted in an over 60% reduction in air travel worldwide according to some estimates. The high economic and public perception costs of potential superspreading during air travel necessitates research efforts that model, explain and mitigate disease spread. The long-duration exposure to infected passengers and the limited air circulation in the cabin are considered to be responsible for the infection spread during flight. Consequently, recent public health measures are primarily based on these aspects. However, a survey of recent on-flight outbreaks indicates that some aspects of the COVID-19 spread, such as long-distance superspreading, cannot be explained without also considering the movement of people. Another factor that could be influential but has not gained much attention yet is the unpredictable passenger behavior. Here, we use a novel infection risk model that is linked with pedestrian dynamics to accurately capture these aspects of infection spread. The model is first parameterized through spatiotemporal analysis of a recent superspreading event in a restaurant in China. The passenger movement during boarding and deplaning, as well as the in-plane movement, are modeled with social force model and agent-based model respectively. We utilize the model to evaluate what-if scenarios on the relative effectiveness of policies and procedures such as masking and social distancing, as well as synergistic effects by combining different approaches in airplanes and other contexts. We find that in certain instances independent strategies can combine synergistically to reduce infection probability by more than a sum of individual strategies.

Dose-response models are widely used to model the relationship between the successful trigger of diseases and the amount of the transmitted dose. There is a wide variation in

infections in transportation-related transmission events, indicating variations in dose potency and threshold. We quantified and bounded viral dose-related parameters using empirical data from transportation-related infection spread events. We then applied the models to parametrically analyze the spread of infection and the effect of mask usage in generic transportation systems. We analyzed five empirical events of SARS-COV-2 transmission where the spatiotemporal details of the infected persons are known. Three common dose response models, the exponential model, the beta-Poisson model, and the Weibull model, were parameterized for these scenarios. This provided parameter ranges corresponding to high, intermediate, and low-dose scenarios. We used these parameter ranges to analyze the spread in generic transportation modes, including a single aisle airplane, bus, and railway coach. We then examined the effect of mask usage and mask quality and performed a PRCC sensitivity analysis of the related factors. The transmission events examined in this study provide a basis for generating high, intermediate, and low-dose model parameterizations. The three dose-response models based on exponential, beta-Poisson, and Weibull distributions adequately reproduced the empirical data with appropriate parameterization. We found that the dose level had a significant impact on the number of secondary infections. In general, mask usage reduced infections at all dose levels. High-quality N-95 masks are effective for all dose levels, while lower-quality masks exhibit a limited mitigation efficiency, especially for high-dose conditions. Sensitivity analysis indicated that the reduction in infection distance threshold is a critical factor in mask usage.

CHAPTER 1: INCORPORATING PEDESTRIAN MOVEMENT IN COMPUTATIONAL MODELS OF COVID-19 SPREAD DURING AIR TRAVEL

1.1 INTRODUCTION

Superspreading events capture public attention and contribute to explosive transmission of infectious diseases. Though there is significant focus on superspreading events in the current COVID-19 pandemic, there have been many prior instances such as Typhoid transmission from asymptomatic individuals in early 20th century [1] and a 2003 outbreak of SARS in Singapore where more than 100 passengers were infected by a flight attendant [2]. A common feature in superspreading events, particularly for COVID-19 is that infectious individuals may be asymptomatic but infective, which makes preventive measures difficult to implement [3].

The chances of superspreading increase in crowded areas [4]. Airtravel often results in crowding of individuals with diverse geographic and immunization backgrounds. Many incidents of infection spread during air travel have been recorded [5], prompting Centers for Disease Control and Prevention (CDC) to suggest guidelines like mask usage onboard airplanes. By studying factors of superspreading events in a well-defined environment like an airplane, not only can we reduce infectious disease spread air travel, one can also understand the efficiency of preventive measures in reducing the infection probability in other contexts.

One reason superspreading events are hard to explain or predict is that the infection pattern itself is a product of complex mechanisms involving factors with high uncertainty, such as human movement behavior, stochasticity in viral exposure during proximate contacts, and

the infectious level of individual. Moreover, proximity based models cannot explain infections that occur beyond contact distance, e.g. infections happening in the rear of airplane when index cases are in the front [4]. Both of these problems can be overcome by introducing pedestrian movement into detailed infection spread models. Aforementioned factors related human behavior and virus transmission can be parameterized in the mathematical models and used to provide insight into a complex superspreading events.

Many researchers have mathematically modeled the pedestrian movement by various methods, for instance, lattice gas model [6], agent-based modeling [7, 8], and cellular automata [9]. Among these, social force model [10, 11] is well developed and has been modified to study various human behaviors, such as panicked evacuation [10], pedestrian motion with information-sharing mechanism [12] etc. We have previously used a modified social force model to evaluate the infection risk during various aspects of air travel [13-16]. Here we combine pedestrian movement model with a dose-response based stochastic infection risk model to analyze infection spread during air travel. The model is parameterized and calibrated by fitting a known superspreading event and parameterized to account for behavioral features such as leaving the middle seat vacant and wearing a mask.

We evaluated our model using a passenger layout of a flight that resulted in a COVID-19 outbreak. Our prior work shows that the model can be used to explain events on a few on-flight outbreaks [17]. Here we utilize the model to parametrically analyze infections spread and mask use effectiveness in a typical single aisle airplane. We also present how the approach could be used in other congregate settings using a movie theater as an example. We show that

our model is able to explain some infection cases that are far away from the infective passenger. Additionally, we quantify how mask effectiveness can lead to variations in infection spread.

1.2 METHODOLOGY

Pedestrian Dynamics

Pedestrians and stationary objects, such as seats, are modeled as particles. Each pedestrian particle comes with a decision-making logic depending on their own situations, such as local pedestrian density and the distance between their current location and the target. The evolution of pedestrian particles accounting for their interactions with other pedestrian particles or wall passengers is computed by Newton's Second Law and integrated from their own velocities, which is described as social force model [11]. The net force $\overline{f_i}$acting on i^{th} pedestrian can be defined as:

$$\overline{f_i} = \frac{m_i}{\tau}\left(\bar{v}_0^i(t) - \bar{v}^i(t)\right) + \sum\nolimits_{j \neq i} \overline{f_{ij}}\,(t) = m_i \frac{d\bar{v}^i(t)}{dt} \quad (1)$$

with pedestrian position at a given time obtained by numerical integration as$\bar{r}^i(t) = \int \bar{v}^i(t)dt$. $\bar{v}_0^i(t)$refers to the desired velocity of pedestrian, and$\bar{v}^i(t)$ that of current velocity. m_i is the particle's mass and τ is the evolution time constant. The momentum,$\frac{m_i}{\tau}\left(\bar{v}_0^i(t) - \bar{v}^i(t)\right)$,is generated by a pedestrian's intention as a part of decision-making, resulting in a self-propulsion force. Addressing the pedestrian's phycology, a repulsion force $\overline{f_{ij}}$(t) is introduced to react to obstacles in the direction of motion and to balance the propulsion term. In this study, we use the Lennard–Jones type repulsion force used earlier by Namilae et al. [13, 16]. Numerical solution of the above ODE for each pedestrian generates a trajectory for each

pedestrian. Additional behavioral features need to be explicitly coded. For example, pedestrians may yield to others as a courtesy or take additional time to load luggage during boarding.

In-flight movement is incorporated for certain activities such as restroom usage and is accomplished by agent-based modeling. Based on the empirical data on in-flight movement [18], we model that 62% of passengers move out of their seats to the closest restroom and return for a median duration of 5.4 minutes. The stochasticity in pedestrian behavior is accounted for by averaging the trajectories over 50 simulations.

Infection Model

Consider the situation in which a susceptible can become infected when in contact with an infected individual for a duration δt. As an initial condition, the model requires insertion of i_c^0 infectives at time zero. The pedestrian dynamics model can be used to estimate the number of susceptibles that come into contact with these infectives for duration δt. The contacts are defined when pedestrians are within a specific transmission distance, which is dependent on the type of pathogen and mechanisms for its spread. For infectious diseases which transmit over longer distances (e.g. 12 ft for COVID-19), it is necessary to incorporate the changes in viral load with distance. This means that the model needs to differentiate between a susceptible at 3 ft distance, who is more likely to be infected, compared to one that is 10 ft away. This can be achieved through a functional form for infection probability of j^{th} susceptible as shown in Eq. 2 below [17].

$$P_j(t) = 1 - \exp\left(-\beta.\delta t \sum_{i=1}^{i_c^0} \left(1 - \frac{r_{ji}}{r_0}\right)^{\alpha}\right) \quad (2)$$

Here r_0 is the threshold distance below which infection transmission is possible, r_{ji} is the distance between infective i and susceptible j. β and α are model parameters. The parameters r_0 , β and α dependent on specific infectious disease and context. The number of secondary infections is then obtained as a summation I(t) = $\sum P_j(t)$ for all the susceptibles.

The infection spread model is parameterized for a superspreading event in a restaurant in Guangzhou, China [19]. The parameter estimation is simpler for this data because the location and status (infected vs susceptible) of all individuals for this event is available. Based on the reported data for the individuals location and infection status, the model parameters are estimated as β = 0.15 minute^{-1}, α= 2.5, and r_0= 3.5 m.

Two primary infection mitigation policies applied in public facilities are social distancing and masking Masks can reduce the level of contagion by decreasing the distance threshold and decreasing the viral dose in the vicinity of the infectious individual, which corresponds to the parameters β and r_0. So far, N-95/FFP2 masks are considered to provide the highest level of protection that can roughly reach at 97% effectiveness in preventing leakage under standard fit [20]. Commonly available over-the-shelf surgical masks are considered to have 50% of filtration efficiency [21]. The distance threshold r_0 is halved to 1.7m for masking scenarios based on a research indicating that the distance of respiratory droplets traveling halves at any given time with surgical mask usage [22]. Incorporating these insights, we studied the effect of masking and social distancing strategies in reducing infection spread in airplanes and other contexts.

1.3 RESULT AND DISCUSSION

We utilized the above model to explain on-flight infection spread in three different air travel related out breaks earlier [17]. We provide the details of our results for one of those flights for completeness followed by a parametric study on relative effectiveness of social distancing and mask use policies. The flight departed from Singapore on January 24th, 2020 and landed in Hangzhou, China on January 25th, with the total flight duration of five hours and 321 passengers on board [5, 23]. There were two diagnosed infective passengers, resulting in 12 secondary infections [5, 23]. Mask usage was mandatory for this flight but quality of masks is unspecified. Given the common usage of cloth and surgical cotton masks, we modeled the condition where all passengers used surgical cotton masks with 50% efficiency of filtration. The exact location of infectious passengers is known apriori. The estimated number of secondary infections from simulations considering passenger movement, is 10.7, which is close to the actual 12 secondary cases reported [23]. Figure 1 shows the infection risk profile as a function of seat.

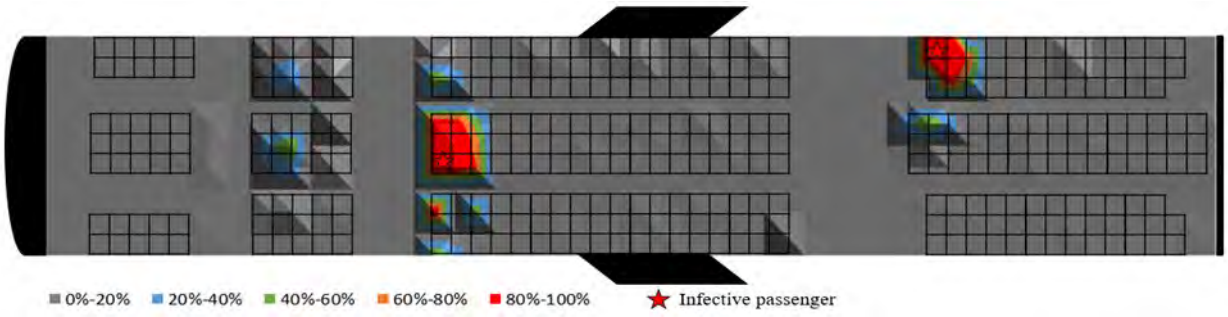

Figure 1. Secondary infection distribution for the Singapore flight for the duration of the flight. Gray indicates the lowest infection risk whereas red indicates the highest risk. Shades within gray contours indicate non-zero infection probability.

We hypothetically examine the spread patterns under no mask usage and high efficiency mask usage. If everyone had used high efficiency N-95 masks for the entire duration of the flight, then the model indicates that there would be 2.3 secondary infections, which is in contrast with 55 secondary infections in a no-mask scenario. The mask efficiency for high quality N-95 masks is considered to be 97%, i.e., 3% leakage, while no-mask case corresponds to 100% leakage. Next, we examine the impact of mask leakages by parametrically varying mask leakage from 3% to 100% (no mask). We also consider various distance thresholds, which could provide insights when the actual distance to which droplets and aerosols travel is known for different airflow and masks. Figure 4 presents these results that could be used to estimate risk when suitable values are identified by future empirical studies for these two parameters. Considering 95% confidence intervals for three scenarios (N-95, surgical and no mask) with 50 simulations each and found that the mean number of infections is 55 cases, 10 cases, and 2 cases, respectively. In both configurations, none of upper and lower bounds of infection overlap, which means each masking scenario clearly has a different impact.

The impact of mask leakages or mask qualities is examined by varying mask leakage from 3% (N-95 with normal fit) to 100% (no mask). We also consider various distance thresholds, which could provide insights when the actual distance that droplets and aerosols travel is known for different airflows and masks. Figure 2 presents these results that could be used to estimate risk if empirical studies identify these two parameters.

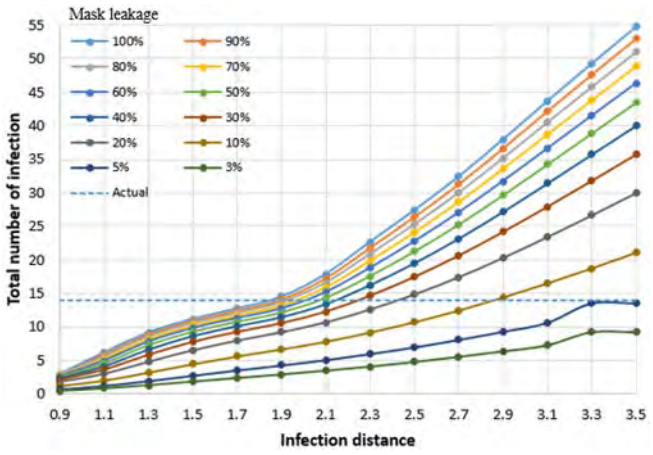

Figure 2. Model results of total infections in the Singapore flight for varying mask leakage and infectivity distance thresholds.

Application to a Generic Airplane

We now examine the synergistical effect of social distancing and masking policy for a generic airplane configuration. We use a seating layout of a single aisle Airbus A-320 aircraft with 157 passengers, and a flight duration of 2 hours. This flight duration and airplane size are representative of common domestic commercial airplanes. The model parameters described earlier were used here as well. A single infective is placed in randomly selected location in the middle of the aircraft. Since the position of the infective is not known apriori, the position is varied across ten different locations and the average infection probability is computed. The infection probability for each passenger and the total number of infections is estimated using equation (2). In response to COVID-19, many airlines had adopted social distancing strategies, such as keeping middle seats vacant, to lower the flight density [24]. A recent study suggested that keeping middle seats empty lowers exposure (dose) significantly [25]. Here, we numerically examine the impact of keeping middle seats vacant on infection risk. Figure 3 (a)

shows the distribution of secondary infections in the airplane with all seats occupied for different levels of mask usage. Thirty infections are observed with no mask usage but this significantly reduces to 0.2 secondary infections when high efficiency masks are used. These numbers reduce to 21 and 0 when the middle seat is kept empty. Figure 4 shows the synergistic interaction between social distancing and masking policy. The relative reduction in the number of infections between a full airplane and one with the middle seat empty for different masking conditions is shown in figure 5. If there is no compounding effect, the efficiency should be uniformly 30% which is the percentage of seats left vacant. The synergistic effect especially with high efficiency masks can be observed from this figure.

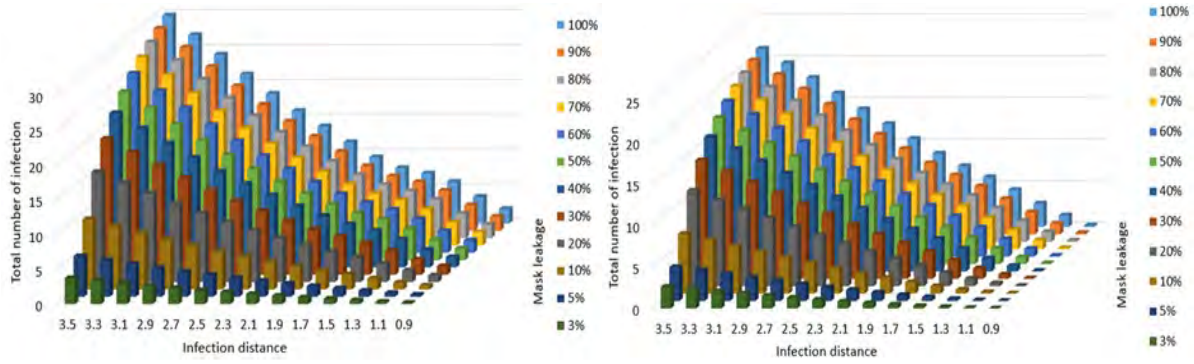

(a) (b)

Figure 3. (a) Model results of the distribution of secondary infections in an A320 airplane for varying mask usage. (b) Distribution of secondary infections with middle seat vacant.

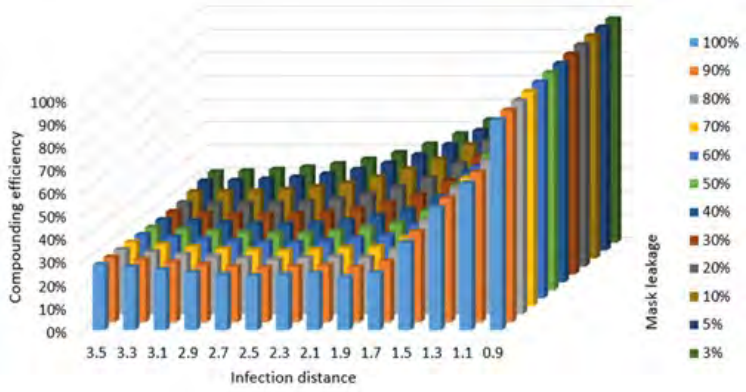

Figure 4. Relative reduction in number of infections comparing middle seat vacant and original aircraft.

To further examine the sensitivity of spread to the parameter variation in Figure 5, the plots exhibit very little change initially (distance 3.5 m), but there is a rapid change in each curve at around 1.7m of infection distance. This indicates that social distancing policy is drastically improved by using masks that reduce the infection distance to 1.7 m or lower.

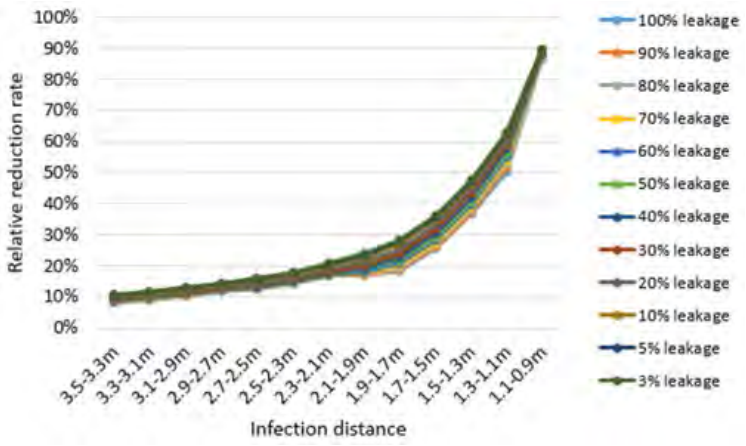

Figure 5. Relative reduction rate of the total number of infections with middle-seat-vacant

Application to Other Contexts – Movie Theater

We now examine if the synergistical effect is dependent on social distancing policy. We use a theater with full capacity of 224 customers as an example, because (i) the scale of population is relatively large so that the synergistical effect may be amplified, and (ii) the scenario is flexible to apply various social distancing patterns. The infective customer is also unknown and assumed to be 1, considering the averaged infective probability of each customer. Social distancing policies applied in the theater are shown in Figure 6 and referred as row wise social distancing, column wise social distancing, and cross social distancing, respectively.

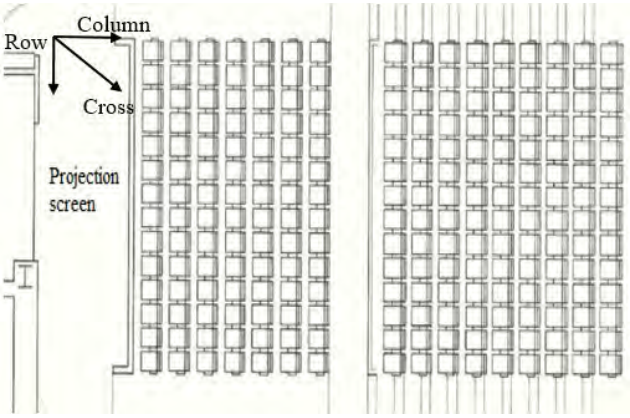

Figure 6. Full capacity of 224 seats in movie theater

All customers are considered stationary during a typical duration of 2 hours. Without social distancing and masks, superspreading infection produces about 16 cases, which is in contrast of 13 cases with only distancing policy applied. The parameter sweep results for various levels of mask usage and social distancing practice are shown in Figure 7 a-d. Low quality masks corresponding to high spreading parameters in figure 8 reduce the infection to a limited extent. Use of high efficiency masks reduces the number of infections to for a full

occupancy case. This is further reduced for the three social distancing strategies. We find that cross seat vacant strategy is more effective especially with high mask usage.

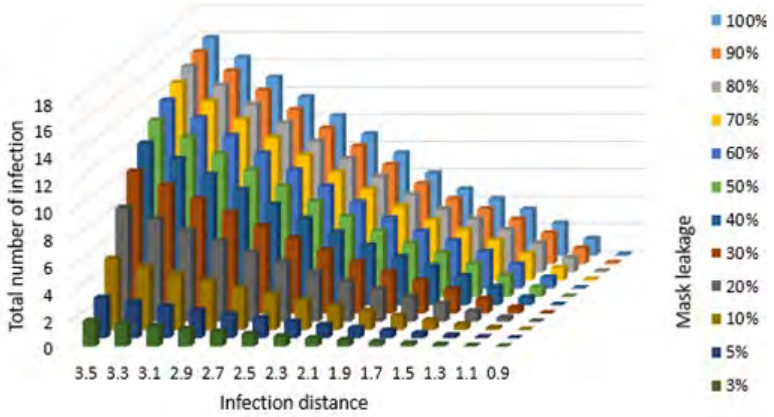

(a)

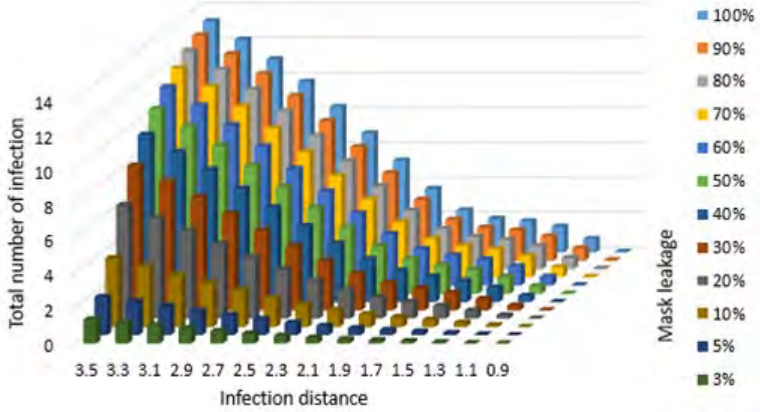

(b)

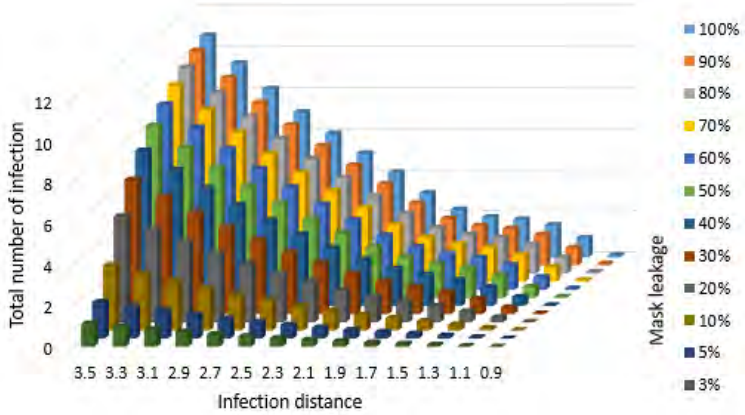

(c)

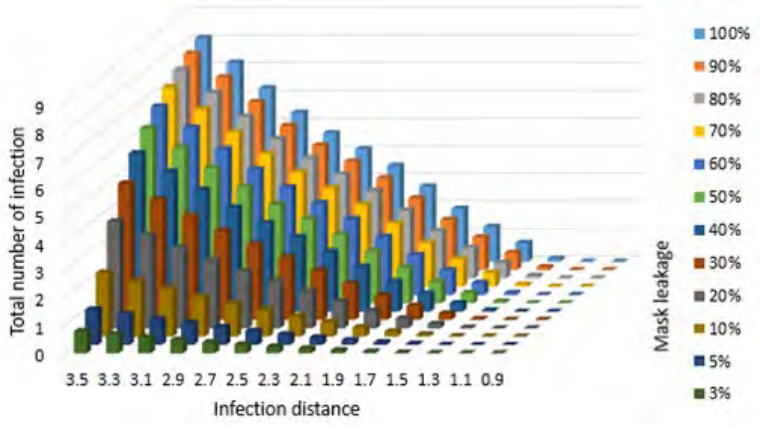

(d)

Figure 7. The total number of secondary infection in theater with (a) full capacity (b) row-wise social distancing (c) column-wise social distancing (d) cross social distancing.

We finally examine the synergistical effect of masks in each social distancing configuration, as shown in Figure 8. Row-wise and column-wise plots present similar behavior in the range of low-quality mask parameters. Figure 8 (c) indicates that cross social distancing has a higher compounding effect over a range of mask efficiency and distance parameters compared to row wise and column wise strategies. There is a clear inflection point in relative reduction of infections when the distance parameter is around 1.7m. This again indicates that social distancing combined with masks that reduce infection radius to 1.7m or lower are most effective in mitigating superspreading events.

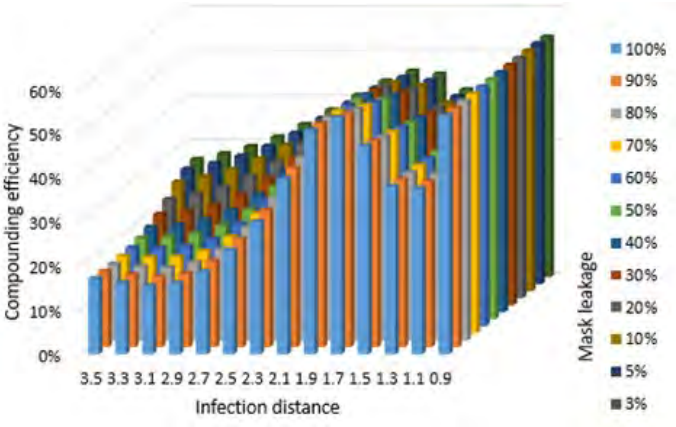

(a)

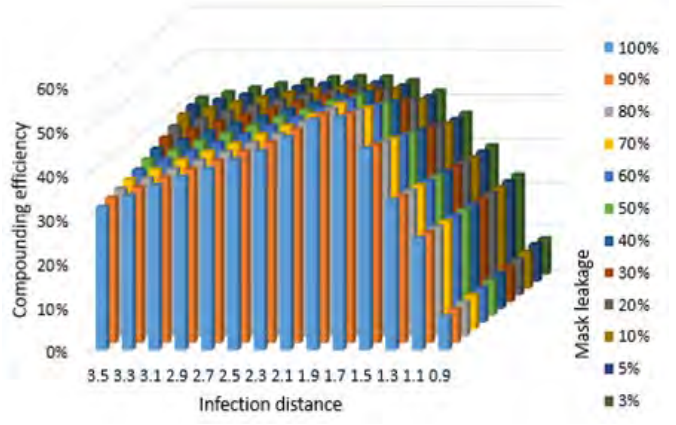

(b)

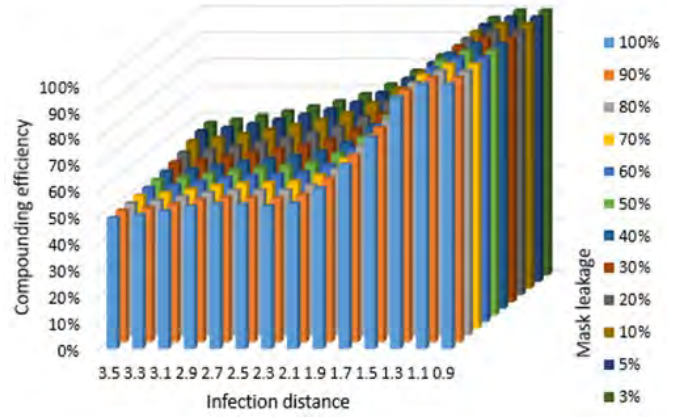

(c)

Figure 8. Synergistical efficiency of masks in (a) row-wise social distancing (b) column-wise social distancing (c) cross social distancing

1.4 CONCLUSIONS

A novel infection risk model combining social-force-based pedestrian dynamics is formulated. The model is used to study the COVID-19 spread pattern in superspreading events incorporating pedestrian movement and is validated by a case study of Singapore flight without mandatory mask usage. The impact of masking is studied by varying the mask filtration efficiency and infection threshold distance. Results suggest that use of high efficiency N-95 or equivalent masks can significantly reduce the risk of secondary infections during a potential superspreading event. Lower efficiency masks also reduce infections but not to the same extant. Social distance policies like keeping the middle seat vacant are not only effective in themselves, the independent masking and social distancing strategies can combine and compound the efficiency of mitigation. We observe a bilinear behavior in relative infection reduction rate with a sudden increase ineffectiveness when masks limit the infection radius to less than 1.7m. The model is generic and can be applied to other crowded areas and such as movie theaters and can be used to suggest effective social distancing approaches.

CHAPTER 2: PARAMETRIC ANALYSIS OF SARS-COV-2 DOSE-RESPONSE MODELS IN TRANSPORTATION SCENARIOS

2.1 INTRODUCTION

There has been significant concern regarding the spread of SARS-CoV-2 on transportation systems. The earliest superspreading events were associated with transportation on cruise ships [26]. Multiple incidents of secondary infection spread have been recorded in various transportation systems including airplanes [23], cruise ships [27], trains [28], and buses [29]. Transportation systems by their very nature involve high-density crowds in relatively small spaces, with limited ventilation. Moreover, geographically diverse groups of people with variations in susceptibility and vaccine use often come together in transportation systems. Early preventative measures often included reducing or stopping air travel and other modes of travel to and from affected regions [30]. Economic disruption in reducing travel can be mitigated to some extent by understanding SARS-CoV-2 spread in transportation systems and designing preventative measures for mitigation. Examples include mask usage mandates, and guidelines aboard airplanes from The Centers for Disease Control and Prevention (CDC) [31] and social distancing approaches such as keeping the middle seat vacant on airplanes [24] Mathematical modeling can be utilized to develop insights into such approaches. For example, using computational modeling, we recently analyzed the relative effectiveness of masks and social distancing in air travel [17;32,33] and effective boarding practices [13,15].

SARS-CoV-2 is primarily transmitted by direct contact with pathogen droplets or aerosols released by a proximate infective person, which correlates with the exposure time and distance between susceptible and infective individuals [34]. A congregation of many people,

such as in transportation systems, combined with a high viral load in the pathogen dose, can result in a high number of secondary infections [35]. While modeling combined with empirical observations is effective in analyzing such infection-spreading events, there are some limitations with respect to both data availability and modeling.

Variations in human behavior with respect to mask usage, social distancing, and personal hygiene lead to a wide variety of situations. This, combined with biological stochasticity, results in vast parameter space. We recently developed algorithms for parameter sweeps that can effectively cover the parameter space with fewer simulations [36, 37]. Empirical data can also help reduce this parameter space. While there are numerous anecdotal instances and news articles on infection spread during transportation, the paucity of contact tracing has limited the data available on infection spread events associated with transportation systems. In this study, we utilized relatively limited empirical data to estimate and bound the parameters related to pathogen dose and its response to proximate susceptibility.

Among the directly transmitted diseases, SARS-CoV-2 can be transmitted over relatively long distances, as high as 12 feet [38]. Therefore, it is necessary for mathematical models to address variations in the viral load with distance. In the context of transportation systems, this means that the models should account for the fact that a susceptible passenger seated 3 feet away is more likely to be infected than one seated 10 feet away. The number of possible infections can be modeled based on the detailed locations and trajectories of individuals and the probability of transmission. In such scenarios, one of the main factors determining whether the infection can be successfully initiated is the amount of pathogen (dose) transmitted from the infected to susceptible individuals [39]. Transmission depends on

the characteristics of pathogens, such as droplet or aerosol dimensions [40], environmental factors such as ventilation, mask usage, and distance between individuals [41], and the duration of exposure [42]. Classical dose-response models are widely used to study such problems by modeling the relationship between the successful trigger of diseases and the amount of transmitted dose. Several dose-response models [43-45] estimate the probability of infection for susceptible individuals that are spatially located in the proximity of infective individuals. Given the novelty of SARS-CoV-2 and unique considerations in transportation systems, these models and empirical data need to be analyzed to find an adequate model and corresponding parameter ranges.

Researchers use infection models in general and dose-response relationships in particular for different types of modeling purposes: (i) descriptive or causal models that explain the mechanisms of a past infection outbreak, (ii) predictive modeling of potential outbreaks, and (iii) prescriptive models that guide interventions. For descriptive or causal models, one would fit the model to the infection outbreak data and examine if the best parameter choice explains the result adequately. For predictive models, one would use a validated model and model parameters for predicting an outbreak in a new situation. For prescriptive purposes, one would generate a variety of possible scenarios and identify interventions that are effective under all these scenarios, so that the intervention is robust against the inherent uncertainties due to biological stochasticity and human behavior. This would require identification of a set of models and parameters that yield different outcomes in the absence of the intervention so that we have a rich set of possible scenarios to evaluate.

In this chapter, we: (a) Quantify the viral dose-related parameters in transportation scenarios by analyzing empirical data from related infection spread events. (b) Compare the various dose-response models and assess their applicability in transportation scenarios. (c) Apply the validated models to parametrically analyze the spread of infection and the effect of mask usage in generic transportation modes, including airplanes, trains, and buses.

2.2 METHODOLOGY

Dose Response Models

Consider a situation with *M* infectious individuals in a total population of *N* individuals with the potential for close proximity contact. When an infective individual i_M and susceptible individual j_N are considered to be in contact, the amount of dose d transmitted during the contact duration (Δt) can be computed as:

$$d(\Delta t)_{j_N,i_M} = \beta \cdot \Delta t \cdot \sum_{i_0}^{M} (1 - \frac{r_{ji}}{r_{thr}})^{\alpha} \quad (1)$$

where β defines the infectivity of the pathogen (probability of successful pathogen transmission per contact), and r_{ij} is the actual distance between two individuals. The variable r_{thr} is the threshold distance beyond which infection is not transmitted. The variable α is the deterioration rate of the pathogen within the spreading radius, and β defines the infectivity of the pathogen.

Susceptible individuals with similar exposure to the dose respond differently because of the biological stochasticity and variations in the vulnerability and receptivity of individuals. The probability of infection for a given exposure to dose (d) was modeled using the

mathematical abstractions listed in Table 1. There have been many applications of dose-response models for the quantitative evaluation of disease transmission from sources, such as sewage, polluted animals, and pathogen-containing aerosols [46-48]. Previous studies have compared the effectiveness of these models, such as the dose-response accuracy [49] and modeling simplicity [50] for various diseases using known biomedical data. However, the application of these models to SARS-CoV-2 has been limited because of the novelty of the virus. Watanabe et al. [49] developed the parameters for an exponential dose-response model for the SARS-CoV outbreak in the early 2000's using datasets of infected mice to analyze the outbreak in a Hong Kong apartment complex. Zhang and Wang [51] evaluated the effect of aerosol transmission viral load on the infection risk of SARS-CoV-2 using an exponential model. Parhizkar et al. [52] developed an infection risk assessment platform with an exponential model in which the estimation suggested a reasonable match with available metadata from outbreaks. Here, we formulate an infection risk model based on previously established dose-response relations and parameterize it using infection spread scenarios in transportation contexts.

Table 1. Mathematical formulations used for dose response models

Model	Formulation	Parameter interpretation	Reference
Exponential	$P(d) = 1 - exp(-rd)$	r: probability for one pathogen cell to trigger a response	[53]
Beta-Poisson	$\mathrm{P}(d) = 1 - (1 + \frac{d}{b_2})^{-b_1}$	b_1:pathogen infectivity; b_2: statistical parameter (shape)	[54,55]
Weibull	$P(d) = 1 - exp(-q_1 d^{q_2})$	q_1: pathogen infectivity; q_2: statistical parameter(shape)	[56,57]
Log-logistic	$\mathrm{P(d)} = \frac{1}{1 + exp[q_1 - q_2 ln(d)]}$	q_1: pathogen infectivity; q_2: statistical parameter(shape)	[58]
Log-Probit	$\mathrm{P(d)} = \Phi\left(\frac{1}{q_2}\ln\left(\frac{d}{q_1}\right)\right)$, where $\Phi(\mathrm{y}) = \frac{1}{\sqrt{2\pi}} \int_{-\infty}^{y} exp(-\frac{x^2}{2})\ \mathrm{dz}$	q_1: pathogen infectivity; q_2: statistical parameter(shape)	[58]

Among these models, the exponential and beta-Poisson models are two commonly used mathematical models, whereas the Weibull model is an effective empirical model [59]. In the exponential model, the pathogen infectivity parameter r is often assigned a fixed value to represent the probability of successful transmission triggered by a single-shot dose [53]. The beta-Poisson model is usually considered an extension of exponential model, where the

pathogen infectivity follows a Γ-distribution instead of a fixed value [53]. For simplicity, the beta-Poisson model is generally approximated in the format shown in Table 1, with numerical requirements of $b_2 \gg 1$ and $b_2 \gg b_1$ [60]. Further, the values of b_1 and b2 can be bounded as $0.05 < b_1 < 2$ and $b_2 > (22b_1)^{0.5}$ to cover many modeling studies [61]. The Weibull model defines infectivity using a Weibull distribution and has been widely used as an empirical model to fit the available data for diseases such as influenza (A/H1N1 2009) [62] and respiratory cancer.

In this study, we parameterized the exponential, beta-Poisson, and Weibull models using the transmission events described in the following section *Parameterization Contexts*. The models were then used to study the spread of infection in generic transportation scenarios with varying doses and mask usage levels.

Parameterization Contexts

To parameterize the dose-response models to specific events of SARS-CoV-2 spread, details of the location of the infectious and infected individuals and duration of exposure are needed. While there are numerous studies that provide overall information on the number of infections, relatively few studies include detailed location maps. These events were used to parameterize the dose-response parameters in Equation (1) and Table 1. Four of these events occurred in the transportation context. Additionally, we included one well-studied infection event at a restaurant. A gathering at a restaurant in Guangzhou, China was identified as a superspreading event, where one known infective customer resulted in 4 to 5 secondary infections with an exposure duration of one hour [19]. The event occurred in the early stages

of the pandemic; therefore, there was no mask usage. The data for the position of each individual in the restaurant, duration of exposure, and infection status before and after the event are documented in Lu et al. [19].

The second event we considered was a ten-hour flight from London to Hanoi on March 1, 2020, with 201 passengers onboard [63]. One infectious individual seated in the first class resulted in 14 secondary infections in the aircraft, 12 were seated in close proximity to the index case in the first class section and two were in the economy cabin. Again, there was no mask usage on this flight.

The third and fourth events involve the same index case: traveling first on a larger bus and then on a mini-bus near Wuhan, China [64]. The larger bus contained 48 passengers onboard and 9 secondary infections were found after a 2.5-hour travel period, among which 8 infections were identified directly related to the trip whereas one infection was suspected to be infected elsewhere. This was followed by a one-hour trip in a mini-bus with 12 passengers, which resulted in two secondary infections. There was no mask usage in any of these cases.

The fifth event is the multistage transmission of infection on a train starting from Harbin, China [65]. The first stage of infection involves 110 minutes of exposure, which results in secondary infections. The second stage involves two secondary infections with 160 minutes of exposure from the same two index cases. There was no temporal overlap between the two infection events. These two events provided an infectivity range for the same index cases. Figure 9 schematically shows the location of the index case and secondary infections for these five events.

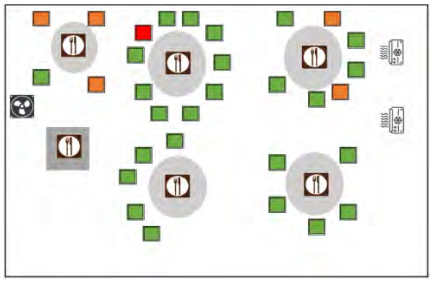

(a)

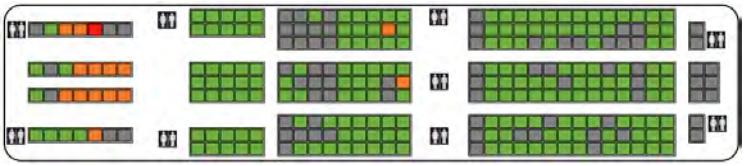

(b)

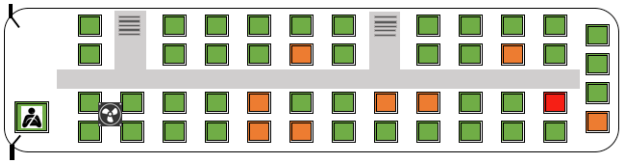

(c)

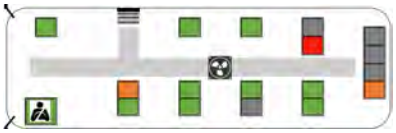

(d)

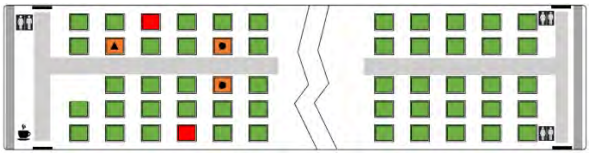

(e)

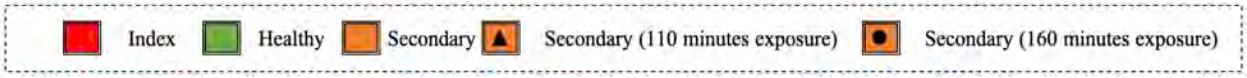

(f)

Figure 9. Schematic infection maps of (a) Guangzhou restaurant (b) UK flight (c) Wuhan large bus (d) Wuhan mini-bus, and (e) Harbin train used for parameterization (f) legend label [19; 63-65]

The exponential model was parameterized using these events. The distance between the index case and susceptible individuals was obtained from the location data. Contact is considered to occur when the distance between two individuals *(r_{ij})* is less than r_{thr}. We vary the values of α, β, and r_{thr} iteratively to compute the infection probability of each susceptible individual. The sum of the infection probabilities provides the total number of infections for a given event. The model parameter set ($\widehat{\Theta}$) that produces the correct number of total infections within tolerance and predicts high probabilities for actual secondary infections are acceptable parameter values as shown in equation 2 below.

$$\widehat{\Theta} = min_{\Theta}\left(N_{observed} - N_{\mathrm{mod}\,el}\right) \tag{2}$$

Beta-Poisson and Weibull models were fitted to each event using the same methodology. The b_1, b_2 parameters in the beta-Poisson model, and the q_1, q_2 parameters in the Weibull model describe the probability distribution for a given dose. These parameters were adapted from a previous computational study on SARS-CoV-2 transmission [66]. The parameters related to the dose, namely, α, β, and r_{thr} were obtained by fitting the model to the data from the aforementioned events. It has been observed that suspended SARS-CoV-2 droplets can be collected up to four meters away from an index person [67]. The value r_{thr} is varied within a limited range based on physical considerations of the aerosol and particle spread.

Application to Transportation Scenarios

We then applied the dose-response models to three generic transportation modes (Figure 9) including a:

- A two-aisle airplane modeled with a layout similar to Airbus A320 aircraft, with 157 passengers including 16 in the business cabin and 141 in the economy cabin. The total

duration of the flight was simulated to be two hours, which corresponds to common regional flights.

- A bus with a similar layout as Greyhound bus, with 52 passengers and one driver. We used a duration of two hours to be consistent with airplane case.
- A railway coach with a seating layout based on Amtrak passenger coach with 61 passengers uniformly seated facing the direction of movement of the train. A two hour duration is used here as well.

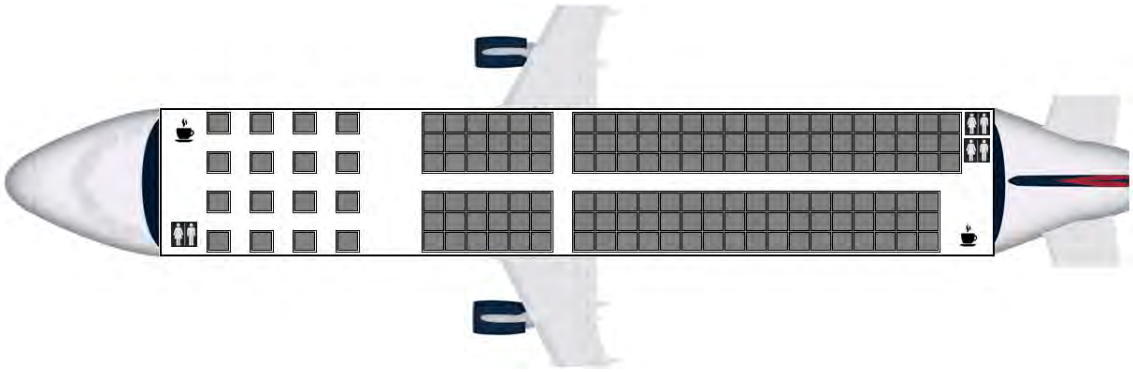

(a)

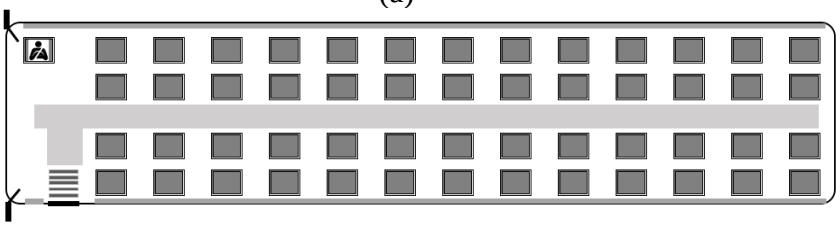

(b)

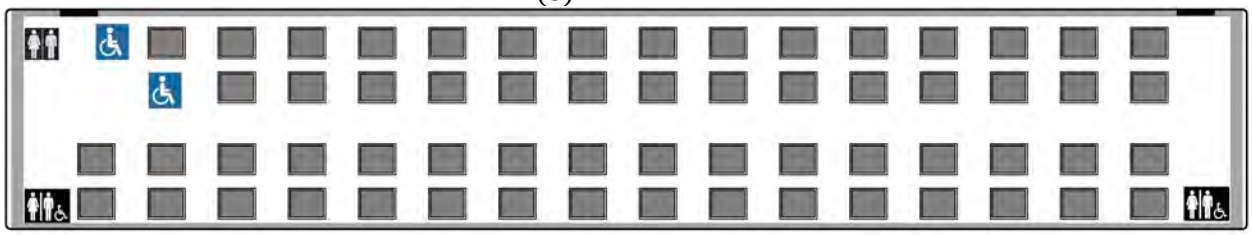

(c)

Figure 9. Schematic of modeling scenario of a generic (a) single aisle aircraft, (b) bus (c) railway coach

In our earlier work, we incorporated the effect of pedestrian movement on the spread of infectious diseases [13-17]. We found that pedestrian movement such as the boarding and

deplaning of an aircraft can explain some empirical observations regarding the location of infected passengers [17]. However, the primary contribution to secondary infections was the colocation of passengers in proximity over an extended period of time. In our five transportation scenarios studied in this current work, we focused on dose variation; therefore, we do not consider the effect of pedestrian movement. Our model methodology can be easily extended to incorporate human movement in future studies.

We also model the impact of mask usage. Note that all the parameters obtained by model fitting are for transmission events with no mask usage. With the application of masks, pathogens can be filtered so that the amount of pathogen dose and range of spread are lower depending on the mask quality. We reduced the parameters β and r_{thr} in equation (1) by a factor corresponding to the mask quality to simulate mask usage. For example, studies have indicated that high-quality N-95 masks with a normal fit are approximately 97% effective in preventing leakage [68]. Cloth masks, such as cotton bandanas "folded surgeon's general style", have a filtration efficiency of up to 50%. In addition, reports indicate that the distance traveled by respiratory droplets is halved with the use of surgical masks [22]. Based on these studies, we performed parameter sweeps to investigate the influence of mask usage on the spread of infection.

2.3 RESULTS AND DISCUSSION

Parameterization of Dose Response Models

The parameter values for the five different events for the three models are summarized in Table 2. Although the Wuhan large bus and the mini-bus event have the same index case,

the layout of susceptible individuals is different, therefore they are separate events. For the Harbin train, one infection transmission occurred during a 110-minute part of the journey, with two more infections occurring in a separate 160-minute portion of the train ride, with the same index cases. The parameterization in Table 2 is based on the 110-minute portion of the train journey. As mentioned earlier, the b_1, b_2 parameters in the beta-Poisson model, and the q_1, q_2 parameters in the Weibull model were adapted from a previous study on SARS-CoV-2 transmission [66]. These parameters describe the shape of the probability distribution for a given dose. The values shown in Table 1 correspond to parameterization that satisfies the total number of infections and give a high probability of infection for the actual cases. Furthermore,

Table 2. Model fitting parameters from available superspreading events

Model Parameterization	Guangzhou Restaurant [19]	UK flight [63]	Wuhan Large bus [64]	Wuhan Mini bus [64]	Harbin Train [65]
Exponential	α=2.5 β=0.15 r_{thr}=3.5m	α=2.4 β=0.2 r_{thr}=3.5m	α=3.3 β=0.02 r_{thr}=3.5 m	α=3.8 β=0.03 r_{thr}=3.5m	α=6.3 β=0.007 r_{thr}=2m
Beta-Poisson	α=1.6 β=1.45 r_{thr}=3.5m $b_1 = 2.27$ * $b_2 = 50.13$*	α=1.6 β=1.4 r_{thr}=3.5m $b_1 = 2.27$ * $b_2 = 50.13$*	α=3.6 β=0.6 r_{thr}=3.5m $b_1 = 2.27$ * $b_2 = 50.13$*	α=2.9 β=0.5 r_{thr}=3.5m $b_1 = 2.27$ * $b_2 = 50.13$*	α=2.5 β=0.06 r_{thr}=2m $b_1 = 2.27$ * $b_2 = 50.13$*
Weibull	α=0.53 β=1.5 r_{thr}=3.5m $q_1 = 0.003 *$ $q_2 = 1.323 *$	α=1.2 β=1.45 r_{thr}=3.5m $q_1 = 0.003 *$ $q_2 = 1.323 *$	α=2.9 β=1.5 r_{thr}=3.5m $q_1 = 0.003 *$ $q_2 = 1.323 *$	α=2 β=1.45 r_{thr}=3.5m $q_1 = 0.003 *$ $q_2 = 1.323 *$	α=2.2 β=0.3 r_{thr}=2m $q_1 = 0.003 *$ $q_2 = 1.323 *$

*b_1, b_2, q_1, q_2 are obtained by COVID-19 transmission analysis from Furuya [66].

the variation of r_{thr} is bounded based on aerosol and droplet mechanisms [67]. While there are numerous factors such as ventilation and air quality that affect the number of infections, our phenomenological approach here models infection transmission without explicitly considering those mechanistic details. The use of numerous transmission events provides the variation in the range of dose.

The corresponding parameters of each model were further compared based on the amount of dose d generated in each scenario as formulated in Equation 1. There are variations in these parameterizing scenarios, i.e., the event duration, the number of infective individuals. In addition, biological stochasticity and human behavioral factors lead to dose variations. Furthermore, the magnitude of the dose required to replicate the observed empirical data is different for the three models because of the differences in the distribution scales which are dependent on the model parameters. To compare the dose levels between the models and scenarios, we normalized the unit dose (per unit time, per index case) to the UK flight scenario as shown in Table 3. We observed that the Guangzhou restaurant and the UK flight scenario contain the highest level of dose, followed by the Wuhan large bus and mini-bus scenarios, and the Harbin train scenario was the lowest. The ranking of the scenarios is consistent across the three models, with minor variations. Among the three models, Weibull model deviated the most from the other two models.

Table 3. Comparison of the normalized dose *d* in each parameterization scenario

Parameterization		Guangzhou Restaurant [19]	UK flight [63]	Wuhan Large bus [64]	Wuhan Mini bus [64]	Harbin Train [65]
Number of infective		1	1	1		2
Exposure/min		20~73 (average=44)	600	150	60	160
Dose per min per index	Exponential	0.483	1.000	0.198	0.114	0.019
	Beta	0.855	1.000	0.525	0.232	0.049
	Weibull	2.007	1.000	1.215	0.692	0.199

Based on the above analysis, we refer to the dose levels that are related to the Guangzhou restaurant and the UK flight as high dose parameters, the Wuhan large bus and mini-bus as intermediate dose parameters, and the Harbin train as low dose parameters. Next, we proceed to use the parameterization in each of the above contexts to analyze the other scenarios. This provides a hypothetical infection analysis of these scenarios utilizing the dose range ranked previously. In Table 4, the first three rows correspond to modeling the Guangzhou restaurant scenario using parameterizations corresponding to the five scenarios using the three models. Similarly, the next three rows correspond to modeling the UK flight with different parameterizations. The subsequent rows correspond to the other three scenarios. Here, the UK flight and Guangzhou restaurant both correspond to high dose parameters, therefore when the parameters corresponding to one of those scenarios is used to model the other, there is close agreement in the number of infections to the observed data. When either of these parameterizations is used to model the Wuhan bus or Harbin train scenarios, the

number of infections is significantly higher. For example, if the high dose parameters corresponding to the UK flight scenario are applied to the Wuhan bus, the models predict that there would be 16-18 potential infections. Empirical data for this intermediate dose scenario shows eight infections. If the dose in this situation were similar to that of Guangzhou restaurant, the model calculates that there would be 18 infections, and if the dose was lower, corresponding to that of Harbin train, there would be about one new infection. The diagonal of the table corresponds to the results of parameterization of the concerned scenario; therefore, it closely matches the empirical results. This analysis shows that the variation in dose significantly affects the estimation of infections.

Based on the results in tables 3 and 4, we can conclude that the three models based on exponential, beta-Poisson and Weibull distributions adequately reproduce the empirical data with appropriate parameterization. When parameterization based on one scenario is applied to other cases (Table 4), one can observe that exponential and beta-Poison models produce similar results while Weibull model indicates fewer infections especially at higher numbers. This is because the tail of the probability density distribution of Weibull model using the specific scalar and shape parameters is different from that of the exponential and beta-Poisson distributions. The cross validation presented in table 4 suggests that Weibull model can reproduce the parameterizing scenarios but produces outcomes different from exponential and beta-Poisson models in other scenarios. This is critical in the context of prescriptive modeling, where we wish to examine if the different models produce a different set of outputs so that a variety of scenarios would be generated. Next, we apply the models to generic transportation

modes and study the impact of mask usage. In subsequent sections, we present the results using the exponential and Weibull models.

Table 4. Cross-validation of parameters in scenarios

Scenarios and Models		Guangzhou Restaurant [19]	UK flight [63]	Wuhan Large bus [64]	Wuhan Mini bus [64]	Harbin Train [65]
Guangzhou Restaurant (4*)	Exponential	***4.3***	*5.1*	0.7	0.7	1.7
	Beta	***4.0***	*4.0*	0.7	0.9	0.04
	Weibull	***4.0***	1.8	0.5	0.9	0.03
UK flight (12*)	Exponential	*11.3*	***11.9***	5.1	5.0	1.0
	Beta	*12.0*	***12.0***	4.8	5.7	1.1
	Weibull	9.0	***11.8***	5.5	8.2	1.4
Wuhan Large Bus (8*)	Exponential	17.5	18.3	***8.0***	*8.9*	0.8
	Beta	16.7	16.6	***8.0***	*8.6*	1.3
	Weibull	18.1	14.2	***8.1***	10.7	1.3
Wuhan Mini Bus (2*)	Exponential	6.7	7.4	*1.7*	***2.0***	0.3
	Beta	5.8	5.7	*1.8*	***2.0***	0.2
	Weibull	4.8	3.1	*1.5*	***2.0***	0.2
Harbin Train (2*)	Exponential	44.3	48.1	16.9	18.1	***2.0***
	Beta	28.8	28.6	12.9	14.1	***2.0***
	Weibull	12.1	22.7	29.9	27.8	***2.1***

*Actual number of infections

Model Application to Generic Transportation Contexts

The dose level of the infected individual varied from high to low based on the parameterizations described in the previous session. For generic situations the position of the infective individual is not known *apriori*, therefore, we vary the location of the infective individual through all possible positions and found the average number of infections with each dose level (Figure 10). Also shown is the effect of all passengers using a cloth mask and an N-95 mask, compared to a no-mask situation. For all three situations, the highest and fewest numbers of infections are observed from the highest level of dose corresponding to the Guangzhou restaurant and the UK flight parameters, and the lowest level of dose corresponding to the train parameters, respectively. The UK flight corresponded to a two-aisle configuration, and the infective was located in the more spacious first-class cabin. The dose response model suggested that an infective with similar dose level in a more densely packed economy cabin of a single aisle aircraft would generate higher number of infections. If the infective was modeled with low dose train parameters, the number of infections are much lower. Also, mask usage, especially N-95 mask usage significantly reduces the number of infections even with a high dose infective.

Similar trends can be observed for the bus and railway coach as shown in Figure 10 (b) and (c). The number of infections in the railway coach varied from 11 to 1 by varying the dose levels. Using cloth masks reduced the infections to four and using N-95 masks reduced the infections to zero for the high dose infective.

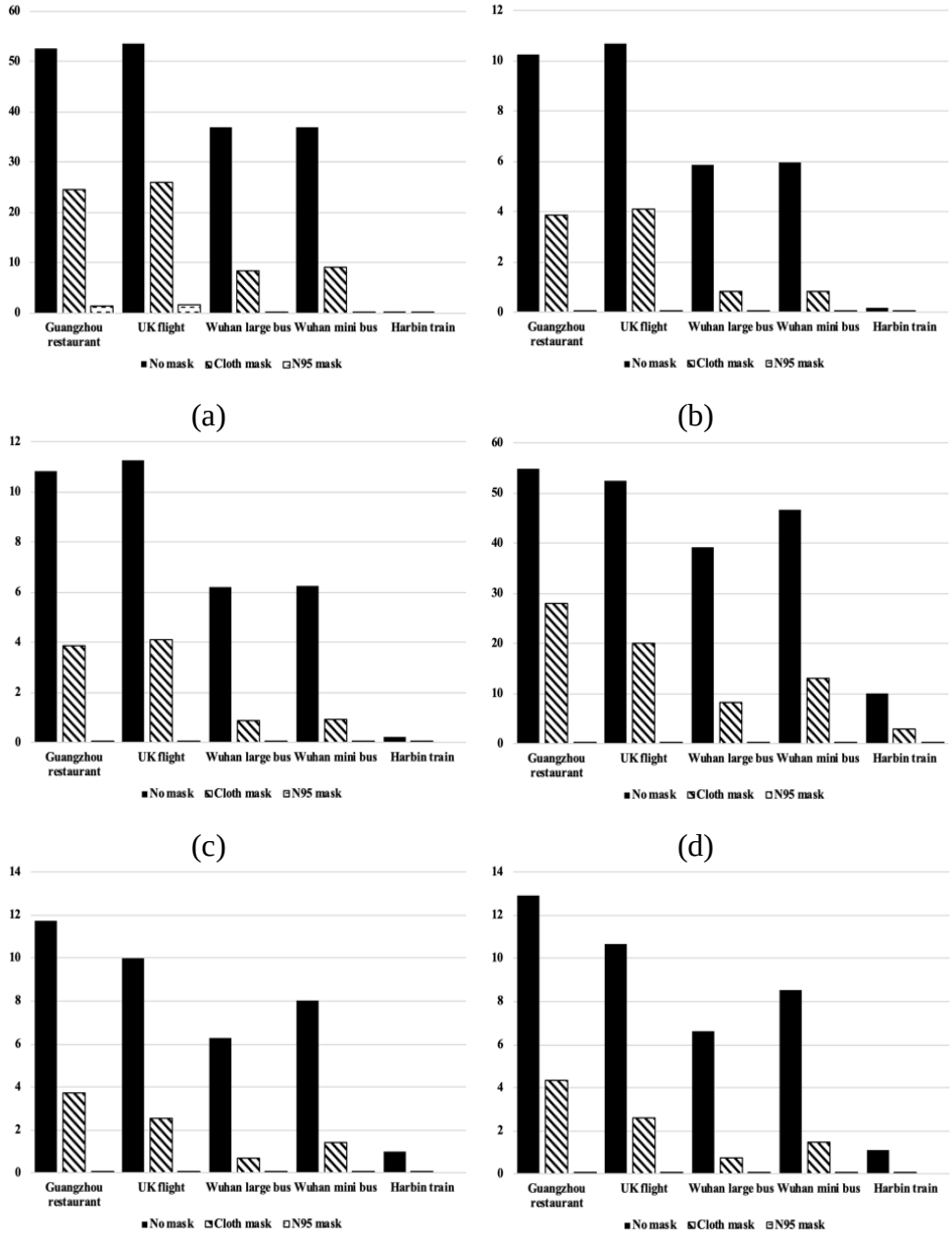

Figure 10. Total infection in (a) single aisle aircraft (b) bus (c) railway coach using the exponential models and in (d) single aisle aircraft (e) bus (f) railway coach using the Weibull models

Parametric Variation

The efficiency of masks varied depending on the mask type, manufacturing quality, and facial fitting. These factors affect the filtration efficiency as well as the distance threshold. A parameter sweep by varying the mask efficiency and distance threshold from a no-mask case to a well-fitting N-95 masks provides a clearer understanding of the role of dose and mask usage in infection spread. Figure 11 shows the parameter variation of mask efficiency and threshold distance for the three cases considered here using high dose (UK flight) parameters. All three cases show a consistent reduction in infections with mask usage, with well-fitting N-95 masks resulting in close to zero infections. Lower quality masks exhibit a limited mitigation efficiency especially for high dose conditions. The reduction in number of infections varies more gradually with improving mask quality in high dose situations (Figure 4) compared to low dose situations.

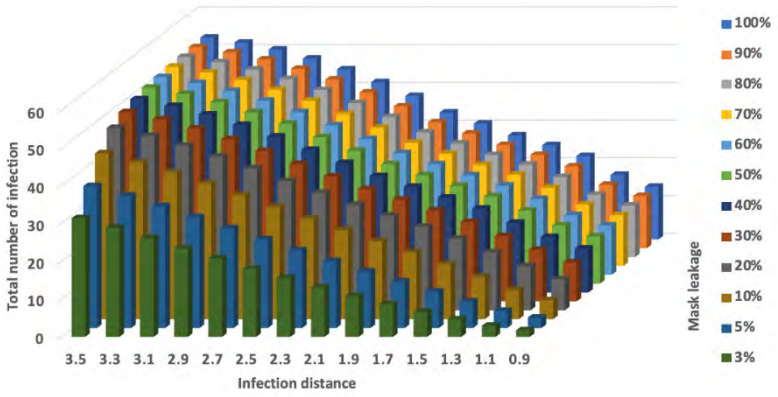

(a)

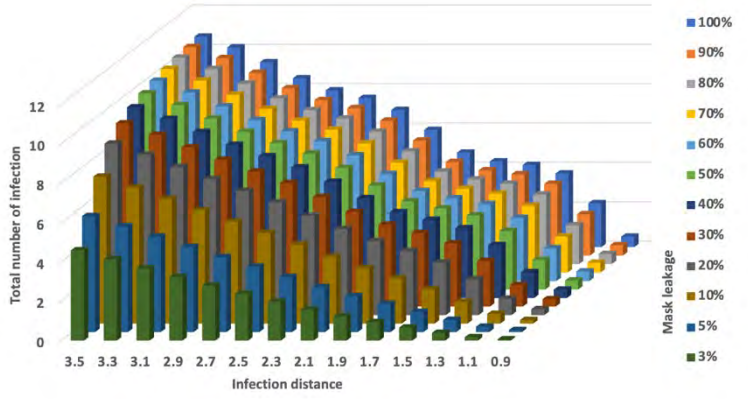
Total number of infection
0
2
4
6
8
10
12
3.5 3.3 3.1 2.9 2.7 2.5 2.3 2.1 1.9 1.7 1.5 1.3 1.1 0.9
Infection distance
Mask leakage
100%
90%
80%
70%
60%
50%
40%
30%
20%
10%
5%
3%

(b)

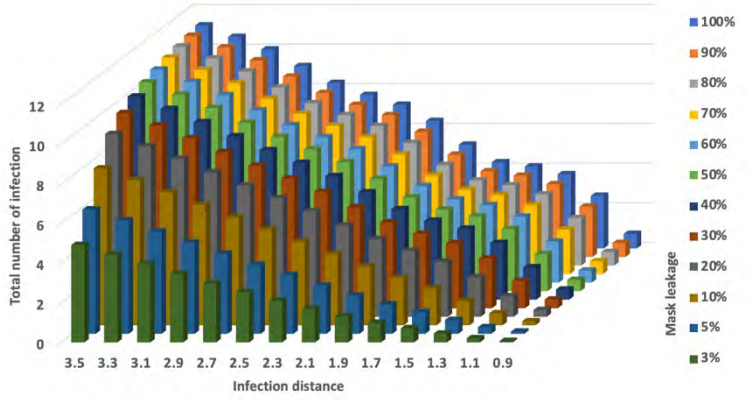
Total number of infection
0
2
4
6
8
10
12
3.5 3.3 3.1 2.9 2.7 2.5 2.3 2.1 1.9 1.7 1.5 1.3 1.1 0.9
Infection distance
Mask leakage
100%
90%
80%
70%
60%
50%
40%
30%
20%
10%
5%
3%

(c)

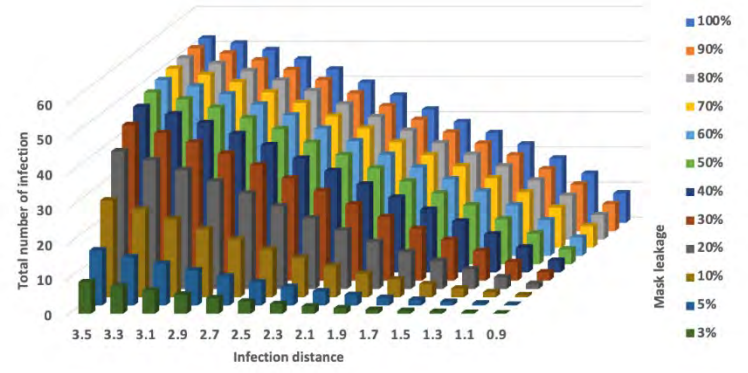
Total number of infection
0
10
20
30
40
50
60
3.5 3.3 3.1 2.9 2.7 2.5 2.3 2.1 1.9 1.7 1.5 1.3 1.1 0.9
Infection distance
Mask leakage
100%
90%
80%
70%
60%
50%
40%
30%
20%
10%
5%
3%

(d)

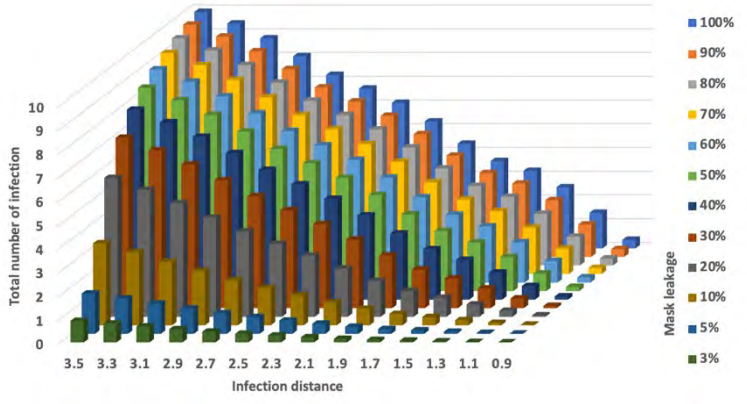

(e)

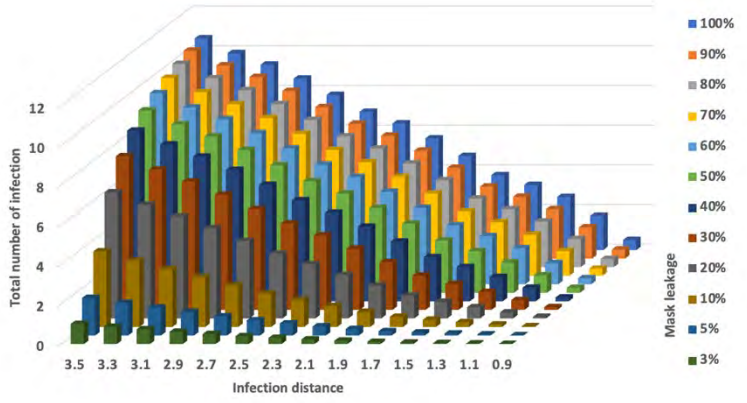

(f)

Figure 11. Parameter sweep with high dose - UK flight parameters using the exponential models for (a) single aisle airplane (b) bus (c) railway coach and using the Weibull models for (d) single aisle airplane (e) bus (f) railway coach

Figure 11 shows the parameter variation with a low dose infective utilizing the Wuhan large bus parameters for the three applications. In contrast with the "convex" shape from the previous high dose application, using the low dose parameters exhibits a concave shape (see Figure 11a). This suggests that lower quality masks can also provide adequate mitigation for low dose situations. Using higher quality masks reduces the number of infections to zero for a significant part of the parameter space as shown in Figure 11 (a). The results follow a similar

trend for beta-Poisson and Weibull dose response models, with Weibull exhibiting difference from the other two models in high infection cases.

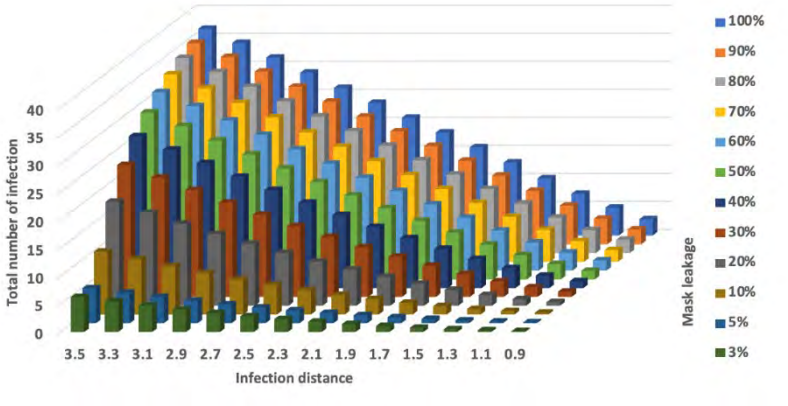

(a)

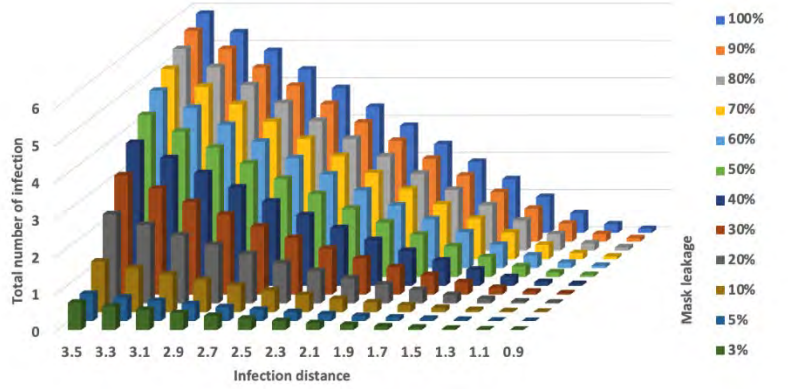

(b)

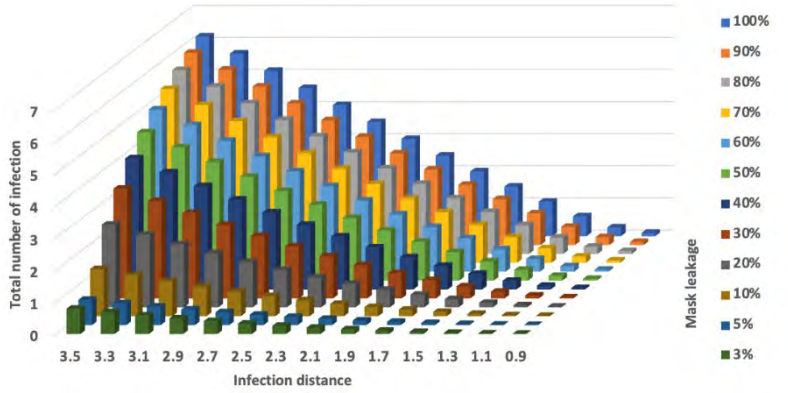

(c)

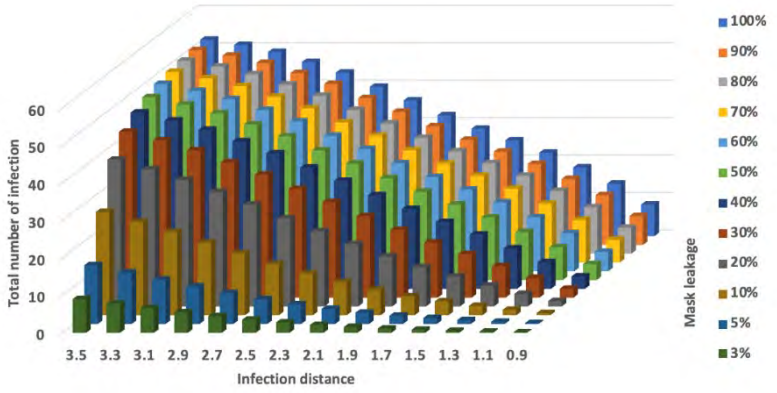

(d)

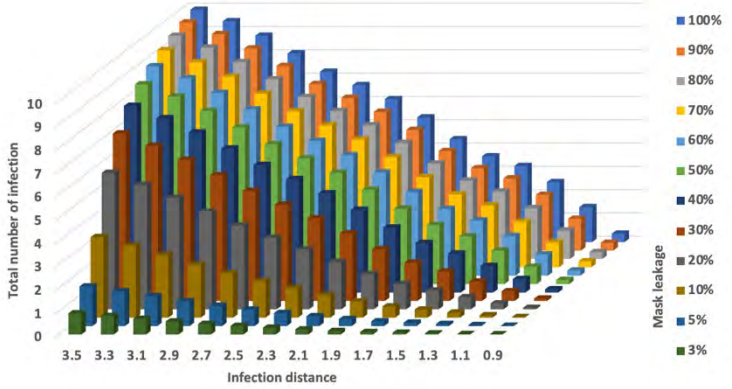

(e)

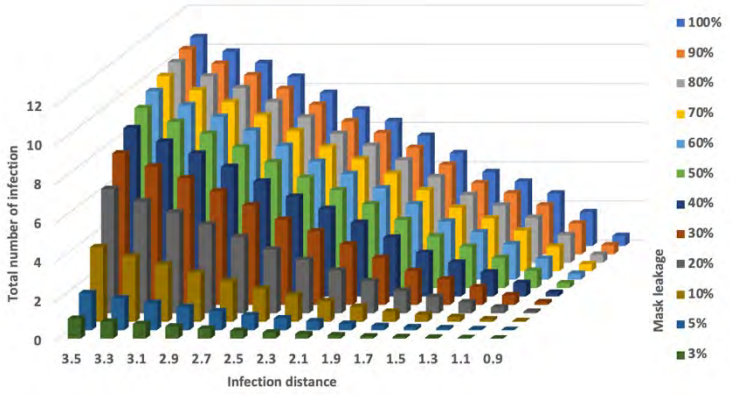

(f)

Figure 11. Parameter sweep with intermediate dose - Wuhan large bus parameters using the exponential models for (a) single aisle airplane (b) bus (c) railway coach and using the Weibull models for (d) single aisle airplane (e) bus (f) railway coach

Sensitivity Analysis

Sensitivity analysis can provide a quantitative perspective on how the infection outcomes of dose response models react to the variation of masking parameters. We used the sampling based Partial Rank Correlation Coefficients (PRCC) sensitivity analysis following the method described in Mubayi et al. [69] and Mubayi [70] to examine (i) which of the two mask related parameters, distance threshold and mask leakage, influence the outcomes more significantly, (ii) how the relative influence of the two parameters varies with dose levels and layout variations. The results shown in Figure 12 indicate that both input parameters have a positive PRCC that is significantly different from 0, with p-values in the range of 10^{-20}~10^{-40}(p-value $\ll 0.05$). This indicates that both parameters have a positive impact on the outcome i.e., there will be a higher infection risk with a larger infection threshold and more mask leakage. A higher value of PRCC indicates greater impact on the outcome. Between the two parameters, infection threshold, with $|PRCC| > 0.9$ at $p < 0.05$ is the more critical parameter in determining the magnitude of infections regardless of the dose levels and seating layouts. The infection threshold possesses a narrower PRCC distribution, whereas the PRCC of the mask leakage varies more widely depending on the dose response model, the dose amount, and the seating layouts. Mask leakage is less influential in high-dose scenarios using Guangzhou restaurant and the UK flight parameterization for all the layouts. Among the seating layouts, mask leakage is less influential in the more densely packed single aisle aircraft configuration. Beta- Poisson and Weibull models also exhibit similar trends.

Comparing between distance threshold and leakage, the higher PRCC for the distance threshold indicates that the effect of masks in reducing the threshold distance resulted in fewer

infections than their effect in reducing the dose itself. PRCC for the mask leakage is lower in the high dose cases compared to intermediate and low dose situations. This suggests that the difference in mask quality is a more significant factor in low dose scenarios compared to high dose cases and larger more densely packed layouts.

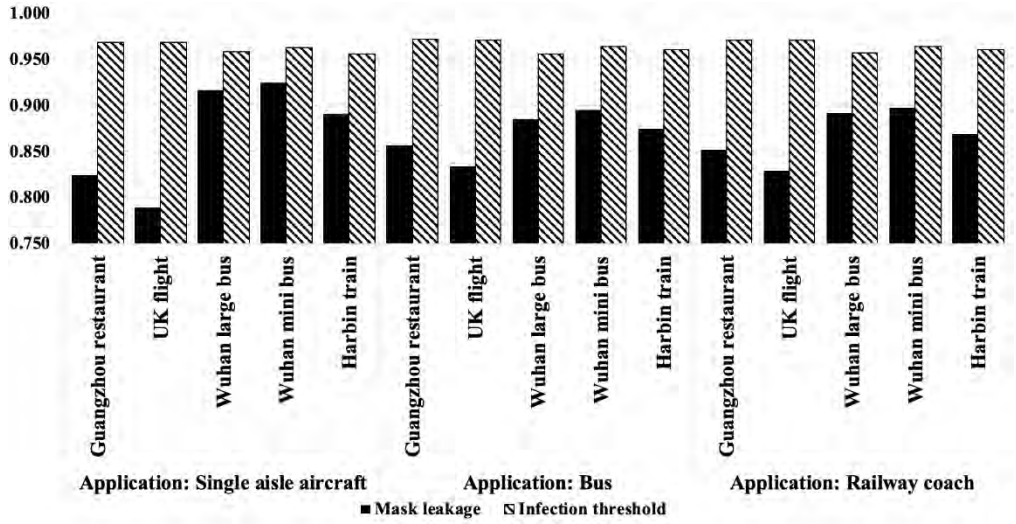

(a)

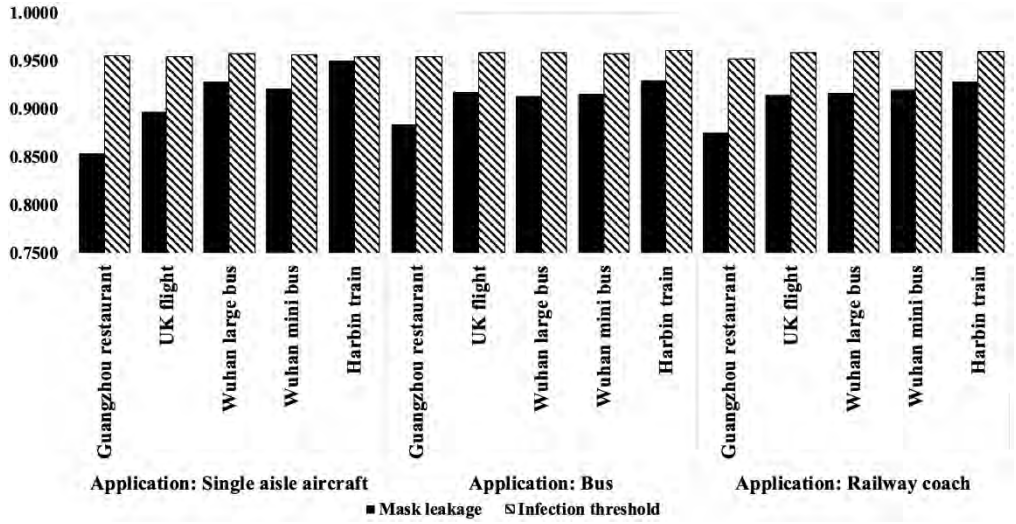

(b)

Figure 12. PRCC of the number of infections in multiple layouts utilizing (a) the exponential models and (b) the Weibull models

Discussion

Despite much literature focusing on SARS-COV-2 transmission, precise quantification of the amount of virions needed to trigger a successful infection is not known. Inherent biological stochasticity combined with differences in intervention usage leads to a wide variation in susceptibility of individuals. Variations in dose levels have resulted in varying outcomes of infection spreading with similar numbers of infective individuals in comparable situations [71]. Understanding and modeling this variability is crucial to effectively model infectious disease spread and for the design of mitigation measures.

Mathematical modeling of multivariate phenomena like infectious disease spread can explicitly account for biological, physical, or social mechanisms through mechanistic modeling. Alternately, phenomenological models extract information from real-world data to help capture the complex causal relationships without requiring the details of the underlying mechanisms. Phenomenological models are especially useful when details (e.g., dose threshold for infection) are not well defined. Here, we use a phenomenological modeling approach and fit different dose-response relations to empirical data of infectious disease spread in transportation. The dose levels in these transportation scenarios vary enabling parametrization of models at different dose levels.

We find that three dose response relations based on exponential, beta-Poisson and Weibull distributions can adequately reproduce the empirical data with appropriate parameterization. Moreover, they exhibit similar trends in parameter sweeps and sensitivity analysis. Weibull model differs from the other two due to the differences in the tails of the distributions.

When modeling is done for prescriptive purposes, e.g., for identify interventions, a large number of scenarios are needed and the intervention needs to be adequate in all (or most) of these scenarios to be considered robust. In addition, it is useful to model extreme situations with high dose parameterization and show that the mitigation measures are effective in such conditions. By using different infection models parametrized to different levels of doses, one can bound the outcomes of hypothetical studies leading to a better understanding. For example, consider the mitigation measure of mask usage. We find that N-95 masks are extremely effective in reducing infection spread in different transportation applications, using different parameterizations and models. Lower quality masks are also effective but for intermediate and low dose scenarios. Sensitivity analysis indicates that the effect of a mask in reducing infection distance threshold is more crucial than in reducing the quantity of the dose itself. Additionally, we find that mask quality has a more significant impact in intermediate and low dose scenarios, compared to high dose case. Transportation systems often involve high-density crowds with diverse levels of intervention use. Our study indicates that high quality mask use is an effective mitigation measure in different transportation modes.

The limitations of our study are as follows. We considered that the infections in the parameterization contexts were caused during the described event (e.g., flight or bus ride). There is a small possibility that contact leading to infection transmission occurred elsewhere. We consider all individuals in these scenarios as stationary. Pedestrian movement within railway coach or airplane can have a small effect on the number of infections. The phenomenological modeling used here does not explicitly account for detailed mechanisms like droplet or aerosol-based spread, or the details of ventilation and airflow, instead these

complex causes are incorporated through empirical data. We also did not consider the effects of vaccination use.

2.4 CONCLUSIONS

We parameterized three common dose-response models with empirical events of SARS-COV-2 transmission to generate model parameters corresponding to high-, intermediate-, and low-dose scenarios. We then used parameterized models to analyze the spread of SARS_COV-2 and the effect of mask usage in generic transportation modes, including a single aisle airplane, bus, and railway coach. We found that dose level had a significant impact on the number of secondary infections. While any mask use reduces secondary infections, high-quality N-95 masks are especially effective. Lower-quality masks exhibit a limited mitigation efficiency, especially for high-dose conditions. The PRCC sensitivity analysis indicated that the effect of masks in reducing the infection distance threshold is a key factor.

REFERENCES

[1] Marineli, F., Tsoucalas, G., Karamanou, M. and Androutsos, G., 2013. Mary Mallon (1869-1938) and the history of typhoid fever. *Annals of gastroenterology: quarterly publication of the Hellenic Society of Gastroenterology*, *26*(2), p.132.

[2] Gopinath, S., Lichtman, J.S., Bouley, D.M., Elias, J.E. and Monack, D.M., 2014. Role of disease-associated tolerance in infectious superspreaders. *Proceedings of the National Academy of Sciences*, *111*(44), pp.15780-15785.

[3] Al-Tawfiq, J.A. and Rodriguez-Morales, A.J., 2020. Super-spreading events and contribution to transmission of MERS, SARS, and COVID-19.

[4] Centers for Disease Control and Prevention, 2021. Scientific Brief: SARS-CoV-2 Transmission. COVID-19, 7 May 2021.

[5] Freedman, D.O. and Wilder-Smith, A., 2020. In-flight transmission of SARS-CoV-2: a review of the attack rates and available data on the efficacy of face masks. *Journal of Travel Medicine*, *27*(8), p.taaa178.

[6] Guo, R.Y. and Huang, H.J., 2008. A mobile lattice gas model for simulating pedestrian evacuation. *Physica A: Statistical Mechanics and its Applications*, *387*(2-3), pp.580-586.

[7] Chen, F., Wang, Z. J., & Zhu, Y. D. (2015, August). Agent-based continuous-space particle pedestrian model. In *Proceedings of the Institution of Civil Engineers-Transport* (Vol. 168, No. 4, pp. 336-345). Thomas Telford Ltd.

[8] Ha, V. and Lykotrafitis, G., 2012. Agent-based modeling of a multi-room multi-floor building emergency evacuation. *Physica A: Statistical Mechanics and its Applications, 391*(8), pp.2740-2751.

[9] Yamamoto, K., Kokubo, S., & Nishinari, K. (2007). Simulation for pedestrian dynamics by real-coded cellular automata (RCA). *Physica A: Statistical Mechanics and its Applications, 379*(2), 654-660.

[10] Helbing, D., Farkas, I. and Vicsek, T., 2000. Simulating dynamical features of escape panic. *Nature, 407*(6803), pp.487-490.

[11] Helbing, D. and Molnar, P., 1995. Social force model for pedestrian dynamics. *Physical review E, 51*(5), p.4282.

[12] Han, Y. and Liu, H., 2017. Modified social force model based on information transmission toward crowd evacuation simulation. *Physica A: Statistical Mechanics and its Applications, 469*, pp.499-509.

[13] Namilae, S., Derjany, P., Mubayi, A., Scotch, M. and Srinivasan, A., 2017. Multiscale model for pedestrian and infection dynamics during air travel. *Physical review E, 95*(5), p.052320.

[14] Derjany, P., Namilae, S., Liu, D. and Srinivasan, A., 2020. Multiscale model for the optimal design of pedestrian queues to mitigate infectious disease spread. *PloS one, 15*(7), p.e0235891.

[15] Islam, T., Lahijani, M.S., Srinivasan, A., Namilae, S., Mubayi, A. and Scotch, M., 2021. From bad to worse: airline boarding changes in response to COVID-19. *Royal Society open science, 8*(4), p.201019.

[16] Namilae, S., Derjany, P., Mubayi, A., Scotch, M. and Srinivasan, A., 2017. Multiscale model for pedestrian and infection dynamics during air travel. *Physical review E, 95*(5), p.052320.

[17] Namilae, S., Wu, Y., Mubayi, A., Srinivasan, A. and Scotch, M., 2022. Identifying mitigation strategies for COVID-19 superspreading on flights using models that account for passenger movement. *Travel Medicine and Infectious Disease, 47*, p.102313.

[18] Hertzberg, V.S., Weiss, H., Elon, L., Si, W., Norris, S.L. and FlyHealthy Research Team, 2018. Behaviors, movements, and transmission of droplet-mediated respiratory diseases during transcontinental airline flights. *Proceedings of the National Academy of Sciences, 115*(14), pp.3623-3627.

[19] Lu, J., Gu, J., Li, K., Xu, C., Su, W., Lai, Z., Zhou, D., Yu, C., Xu, B. and Yang, Z., 2020. COVID-19 outbreak associated with air conditioning in restaurant, Guangzhou, China, 2020. *Emerging infectious diseases, 26*(7), p.1628.

[20] Srinivasan, A., Mubayi, A. and Akman, O., 2020. Should N95 respirators be recommended for the general public. *Letters in Biomathematics, 7*(1), pp.143-152.

[21] Clapp, P.W., Sickbert-Bennett, E.E., Samet, J.M., Berntsen, J., Zeman, K.L., Anderson, D.J., Weber, D.J. and Bennett, W.D., 2021. Evaluation of cloth masks and modified procedure masks as personal protective equipment for the public during the COVID-19 pandemic. *JAMA Internal Medicine, 181*(4), pp.463-469.

[22] Dbouk, T. and Drikakis, D., 2020. On respiratory droplets and face masks. *Physics of Fluids, 32*(6), p.063303.

[23] Yang, N., Shen, Y., Shi, C., Ma, A.H.Y., Zhang, X., Jian, X., Wang, L., Shi, J., Wu, C., Li, G. and Fu, Y., 2020. In-flight transmission cluster of COVID-19: a retrospective case series. *Infectious diseases*, *52*(12), pp.891-901.

[24] Dinges, G., 2020. New Delta Air Lines boarding procedures aimed at preventing spread of coronavirus. USA Today, 11.

[25] Dietrich, W.L., Bennett, J.S., Jones, B.W. and Hosni, M.H., 2021. Laboratory modeling of SARS-CoV-2 exposure reduction through physically distanced seating in aircraft cabins using bacteriophage aerosol—November 2020. *Morbidity and Mortality Weekly Report*, *70*(16), p.595.

[26] Rocklöv, J., Sjödin, H. and Wilder-Smith, A., 2020. COVID-19 outbreak on the Diamond Princess cruise ship: estimating the epidemic potential and effectiveness of public health countermeasures. Journal of travel medicine, 27(3), p.taaa030.

[27] Quigley, A.L., Nguyen, P.Y., Stone, H., Lim, S. and MacIntyre, C.R., 2020. Cruise ship travel and the spread of COVID-19–Australia as a case study. International Journal of Travel Medicine and Global Health, 9(1), pp.10-18

[28] Zhao, S., Zhuang, Z., Ran, J., Lin, J., Yang, G., Yang, L. and He, D., 2020. The association between domestic train transportation and novel coronavirus (2019-nCoV) outbreak in China from 2019 to 2020: a data-driven correlational report. Travel medicine and infectious disease, 33, p.101568.

[29] Shen, Y., Li, C., Dong, H., Wang, Z., Martinez, L., Sun, Z., Handel, A., Chen, Z., Chen, E., Ebell, M. and Wang, F., 2020. Airborne transmission of COVID-19: epidemiologic evidence from two outbreak investigations.

[30] Rahman, M.K., Gazi, M.A.I., Bhuiyan, M.A. and Rahaman, M.A., 2021. Effect of Covid-19 pandemic on tourist travel risk and management perceptions. Plos one, 16(9), p.e0256486.

[31] Centers for Disease Control and Prevention, 2021. Requirement for persons to wear masks while on conveyances and at transportation hubs. DHHS, editor.

[32] Wu, Y., Namilae, S., Mubayi, A., Scotch, M. and Srinivasan, A., 2021. Computational modeling of on-flight COVID-19 spread incorporating pedestrian movement. Journal of Transport & Health, 22, p.101172

[33] Wu, Y., Namilae, S., Mubayi, A., Scotch, M. and Srinivasan, A., 2022, March. Incorporating Pedestrian Movement in Computational Models of COVID-19 Spread during Air-travel. In 2022 IEEE Aerospace Conference (AERO) (pp. 1-8). IEEE

[34] Marín-García, D., Moyano-Campos, J.J. and Bienvenido-Huertas, J.D., 2021. Distances of transmission risk of COVID-19 inside dwellings and evaluation of the effectiveness of reciprocal proximity warning sounds. Indoor air, 31(2), pp.335-347.

[35] Gómez-Carballa, A., Pardo-Seco, J., Bello, X., Martinón-Torres, F. and Salas, A., 2021. Superspreading in the emergence of COVID-19 variants. Trends in Genetics, 37(12), pp.1069-1080.

[36] Derjany, P., Namilae, S. and Srinivasan, A., 2021. Parameter Space Exploration in Pedestrian Queue Design to Mitigate Infectious Disease Spread. Journal of the Indian Institute of Science, 101(3), pp.329-339.

[37] Chunduri, S., Ghaffari, M., Lahijani, M.S., Srinivasan, A. and Namilae, S., 2018, May. Parallel low discrepancy parameter sweep for public health policy. In 2018 18th

IEEE/ACM International Symposium on Cluster, Cloud and Grid Computing (CCGRID) (pp. 291-300). IEEE.

[38] Manigandan, S., Wu, M.T., Ponnusamy, V.K., Raghavendra, V.B., Pugazhendhi, A. and Brindhadevi, K., 2020. A systematic review on recent trends in transmission, diagnosis, prevention and imaging features of COVID-19. Process Biochemistry, 98, pp.233-240.

[39] Kwon, J.S., Kim, J.Y., Kim, M.C., Park, S.Y., Kim, B.N., Bae, S., Cha, H.H., Jung, J., Kim, M.J., Lee, M.J. and Choi, S.H., 2020. Factors of severity in patients with COVID-19: cytokine/chemokine concentrations, viral load, and antibody responses. The American journal of tropical medicine and hygiene, 103(6), p.2412.

[40] Jayaweera, M., Perera, H., Gunawardana, B. and Manatunge, J., 2020. Transmission of COVID-19 virus by droplets and aerosols: A critical review on the unresolved dichotomy. Environmental research, 188, p.109819.

[41] Leder, K. and Newman, D., 2005. Respiratory infections during air travel. Internal medicine journal, 35(1), pp.50-55.

[42] Smieszek, T., 2009. A mechanistic model of infection: why duration and intensity of contacts should be included in models of disease spread. Theoretical Biology and Medical Modelling, 6(1), pp.1-10.

[43] Sun, C. and Zhai, Z., 2020. The efficacy of social distance and ventilation effectiveness in preventing COVID-19 transmission. Sustainable cities and society, 62, p.102390.

[44] Lelieveld, J., Helleis, F., Borrmann, S., Cheng, Y., Drewnick, F., Haug, G., Klimach, T., Sciare, J., Su, H. and Pöschl, U., 2020. Model calculations of aerosol transmission and

infection risk of COVID-19 in indoor environments. International Journal of Environmental Research and Public Health, 17(21), p.8114.

[45] Mittal, R., Meneveau, C. and Wu, W., 2020. A mathematical framework for estimating risk of airborne transmission of COVID-19 with application to face mask use and social distancing. Physics of Fluids, 32(10), p.101903.

[46] Medema, G., Wullings, B., Roeleveld, P. and Van Der Kooij, D., 2004. Risk assessment of Legionella and enteric pathogens in sewage treatment works. Water Science and Technology: Water Supply, 4(2), pp.125-132.

[47] Alarie, Y., 1981. Dose-response analysis in animal studies: prediction of human responses. Environmental Health Perspectives, 42, pp.9-13. \

[48] Sze To, G.N. and Chao, C.Y.H., 2010. Review and comparison between the Wells–Riley and dose-response approaches to risk assessment of infectious respiratory diseases. Indoor air, 20(1), pp.2-16.

[49] Watanabe, T., Bartrand, T.A., Weir, M.H., Omura, T. and Haas, C.N., 2010. Development of a dose-response model for SARS coronavirus. Risk Analysis: An International Journal, 30(7), pp.1129-1138.

[50] Guo, M., Mishra, A., Buchanan, R.L., Dubey, J.P., Hill, D.E., Gamble, H.R., Jones, J.L., Du, X. and Pradhan, A.K., 2016. Development of Dose-Response Models to Predict the Relationship for Human Toxoplasma gondii Infection Associated with Meat Consumption. Risk Analysis, 36(5), pp.926-938.

[51] Zhang, X. and Wang, J., 2021. Dose-response relation deduced for coronaviruses from COVID-19, SARS and MERS meta-analysis results and its application for infection

risk assessment of aerosol transmission. Clinical Infectious Diseases, 73(1), pp.e241-e245.

[52] Parhizkar, H., Van Den Wymelenberg, K.G., Haas, C.N. and Corsi, R.L., 2022. A quantitative risk estimation platform for indoor aerosol transmission of COVID-19. Risk Analysis, 42(9), pp.2075-2088.

[53] Haas, C.N., Rose, J.B. and Gerba, C.P., 2014. Quantitative microbial risk assessment. John Wiley & Sons.

[54] Furumoto, W.A. and Mickey, R., 1967. A mathematical model for the infectivity-dilution curve of tobacco mosaic virus: Experimental tests. Virology, 32(2), pp.224-233.

[55]Furumoto, W.A. and Mickey, R., 1967. A mathematical model for the infectivity-dilution curve of tobacco mosaic virus: Theoretical considerations. Virology, 32(2), pp.216-223.

[56] Christensen, E.R., 1984. Dose-response functions in aquatic toxicity testing and the Weibull model. Water Research, 18(2), pp.213-221.

[57] Christensen, E.R. and Chen, C.Y., 1985. A general noninteractive multiple toxicity model including probit, logit, and Weibull transformations. Biometrics, pp.711-725.

[58] Prentice, R.L., 1976. A generalization of the probit and logit methods for dose response curves. Biometrics, pp.761-768.

[59] Christensen, E.R. and Nyholm, N., 1984. Ecotoxicological assays with algae: Weibull dose-response curves. Environmental science & technology, 18(9), pp.713-718.

[60] Teunis, P.F.M. and Havelaar, A.H., 2000. The Beta Poisson dose-response model is not a single-hit model. Risk Analysis, 20(4), pp.513-520.

[61] Xie, G., Roiko, A., Stratton, H., Lemckert, C., Dunn, P.K. and Mengersen, K., 2017. Guidelines for use of the approximate beta-Poisson dose–response model. Risk Analysis, 37(7), pp.1388-1402.

[62] Spackman, E., Malladi, S., Ssematimba, A. and Stephens, C.B., 2019. Assessment of replicate numbers for titrating avian influenza virus using dose-response models. Journal of Veterinary Diagnostic Investigation, 31(4), pp.616-619.

[63] Khanh, N.C., Thai, P.Q., Quach, H.L., Thi, N.A.H., Dinh, P.C., Duong, T.N., Mai, L.T.Q., Nghia, N.D., Tu, T.A., Quang, L.N. and Dai Quang, T., 2020. Transmission of SARS-CoV 2 during long-haul flight. Emerging infectious diseases, 26(11), p.2617.

[64] Luo, K., Lei, Z., Hai, Z., Xiao, S., Rui, J., Yang, H., Jing, X., Wang, H., Xie, Z., Luo, P. and Li, W., 2020, October. Transmission of SARS-CoV-2 in public transportation vehicles: a case study in Hunan Province, China. In Open forum infectious diseases (Vol. 7, No. 10, p. ofaa430). US: Oxford University Press.

[65] Zhou, L., Yao, L., Hao, P., Li, C., Zhao, Q., Dong, H., Dou, J., Wang, S., Gao, G.F., Li, Q. and Huang, B., 2021. COVID-19 cases sprFead through the K350 train—Jilin and Heilongjiang Provinces, China, January 2021. China CDC Weekly, 3(8), p.162.

[66] Furuya, H., 2020. Prediction of potential respiratory tract infection from SARS-CoV-2 through hand-to-face contact transmission. Tokai J. Exp. Clin. Med, 45, pp.170-175.

[67] Guo, Z.D., Wang, Z.Y., Zhang, S.F., Li, X., Li, L., Li, C., Cui, Y., Fu, R.B., Dong, Y.Z., Chi, X.Y. and Zhang, M.Y., 2020. Aerosol and surface distribution of severe acute respiratory syndrome coronavirus 2 in hospital wards, Wuhan, China, 2020. Emerging infectious diseases, 26(7), p.1586.

[68] Grinshpun, S.A., Haruta, H., Eninger, R.M., Reponen, T., McKay, R.T. and Lee, S.A., 2009. Performance of an N95 filtering facepiece particulate respirator and a surgical mask during human breathing: two pathways for particle penetration. Journal of occupational and environmental hygiene, 6(10), pp.593-603.

[69] Mubayi, A., 2017. Computational modeling approaches linking health and social sciences: Sensitivity of social determinants on the patterns of health risk behaviors and diseases. In Handbook of statistics (Vol. 36, pp. 249-304). Elsevier.

[70] Mubayi, A., Greenwood, P., Wang, X., Castillo-Chávez, C., Gorman, D.M., Gruenewald, P. and Saltz, R.F., 2011. Types of drinkers and drinking settings: an application of a mathematical model. Addiction, 106(4), pp.749-758

[71] Susswein, Z. and Bansal, S., 2020. Characterizing superspreading of SARS-CoV-2: from mechanism to measurement. MedRxiv.

APPENDIX – AIRPORT USAGE DATA FOR THE BUSIEST AIRPORTS IN USA AND CORRESPONDING NUMBER OF COVID-19 CASES

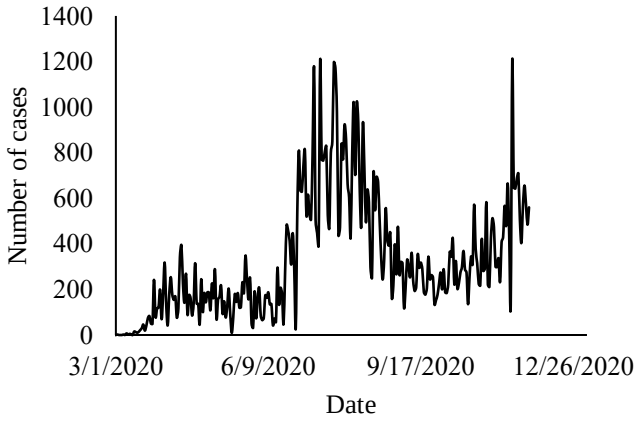

(a)

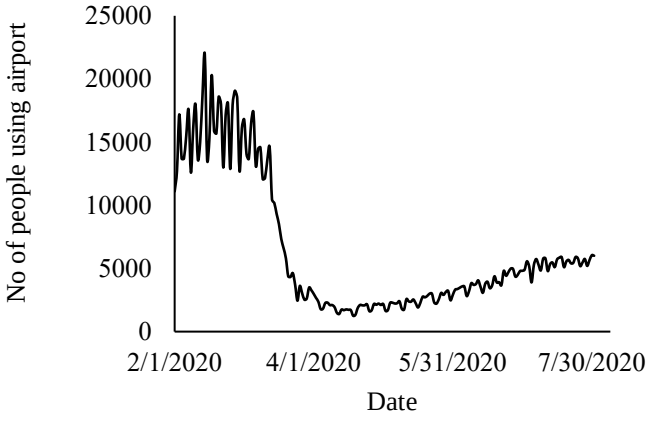

(b)

Figure 13. (a) Number of COVID-19 cases in counties around ATL airport (b) Number of people using ATL airport.

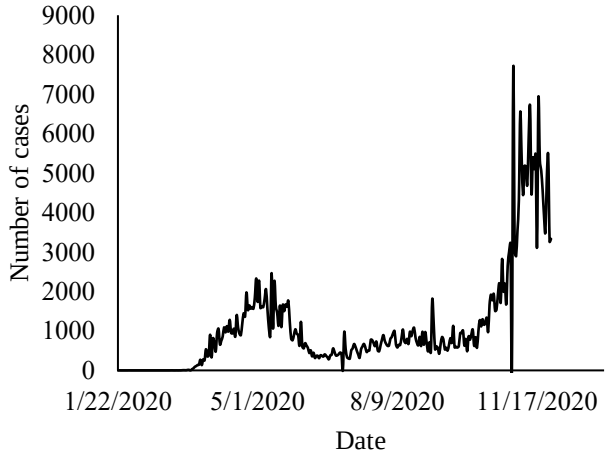

(a)

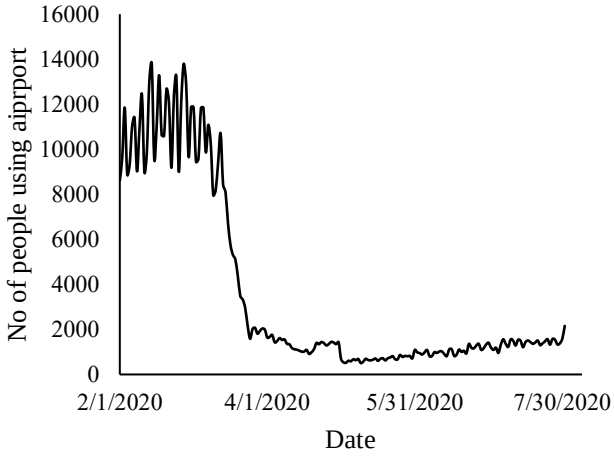

(b)

Figure 14. (a) Number of COVID-19 cases in counties around Chicago ORD airport (b) Number of people using ORD airport.

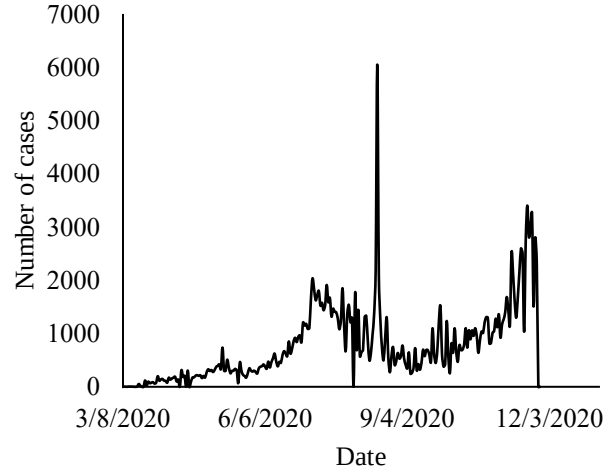

(a)

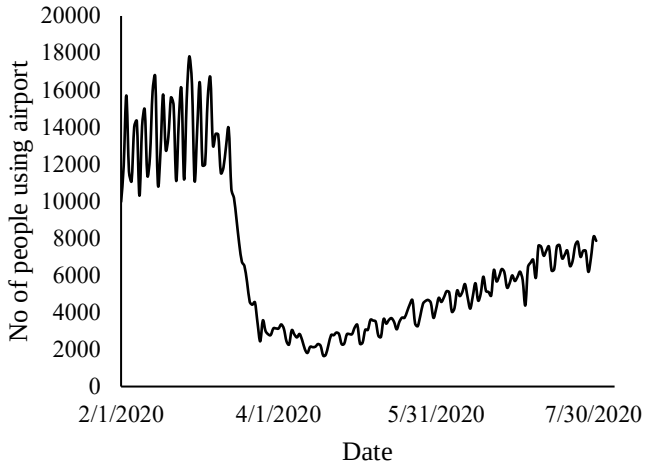

(b)

Figure 15. (a) Number of COVID-19 cases in counties around Dallas DFW airport (b) No of people using DFW airport.

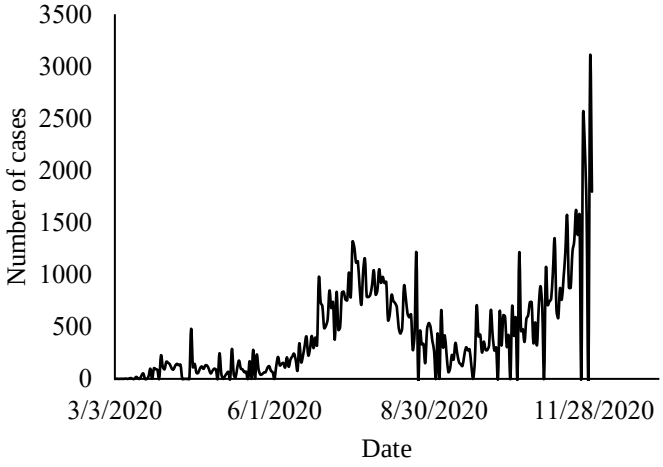

(a)

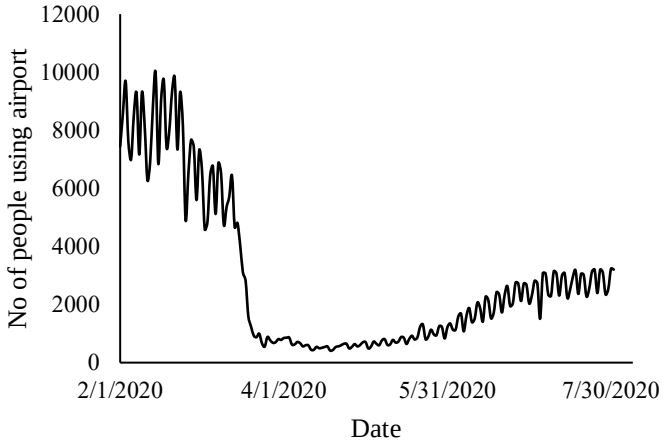

(b)

Figure 16. (a) Number of COVID-19 cases in counties around Las Vegas LAS airport (b) No of people using LAS airport.

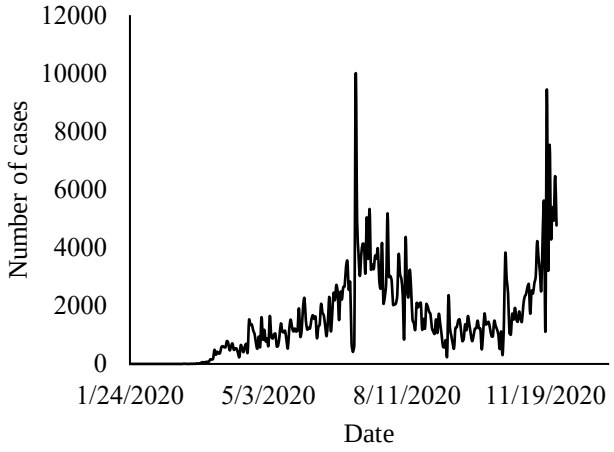

(a)

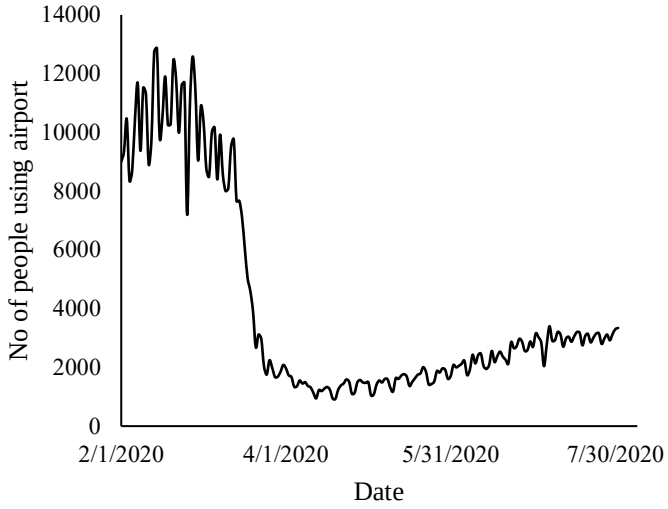

(b)

Figure 17 (a) Number of COVID-19 cases in counties around Los Angles LAX airport (b) No of people using LAX airport.

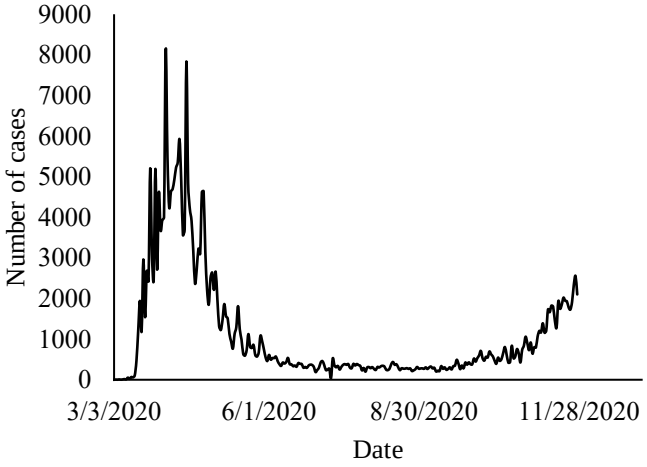

(a)

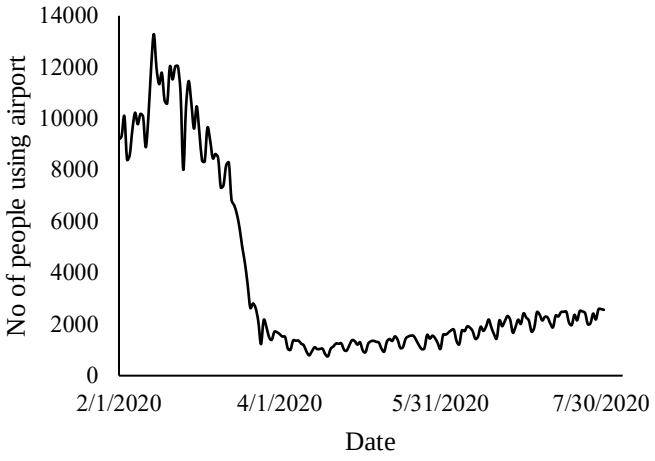

(b)

Figure 18 (a) Number of COVID-19 cases in counties around New York JFK airport (b) No of people using JFK airport.

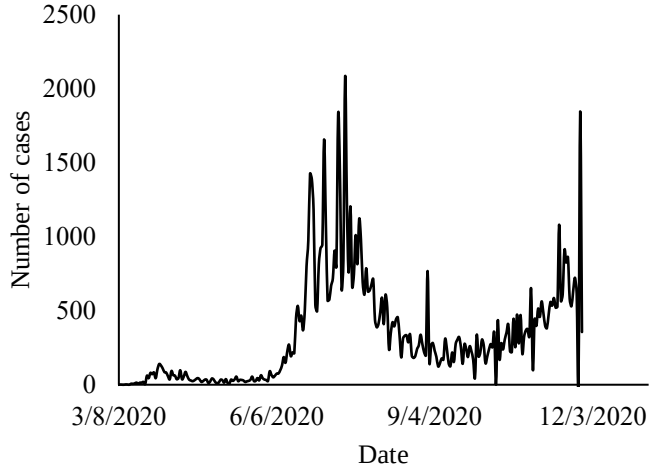

(a)

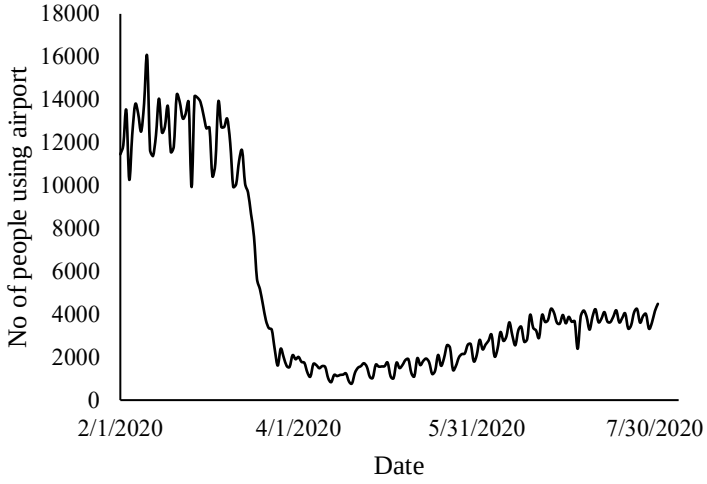

(b)

Figure 19 (a) Number of COVID-19 cases in counties around Orlando MCO airport (b) No of people using MCO airport.

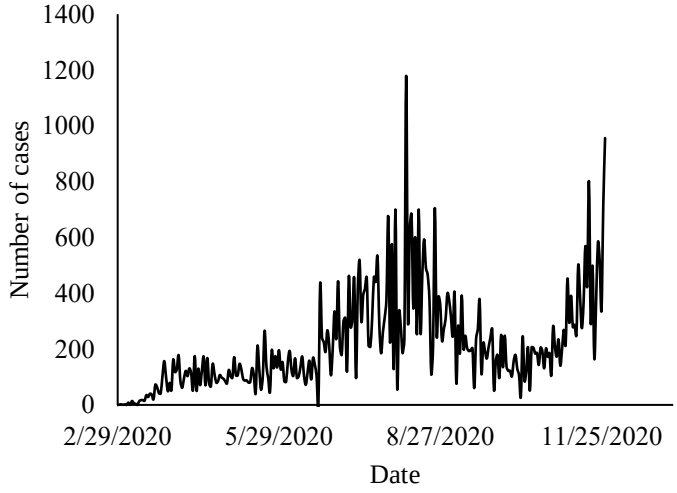

(a)

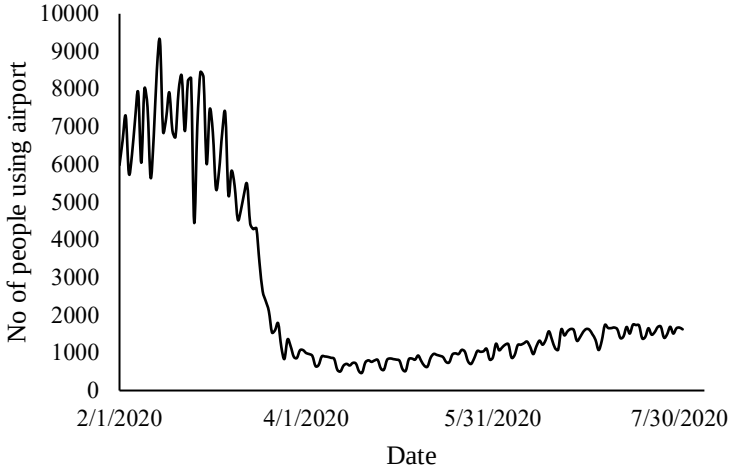

(b)

Figure 20 (a) Number of COVID-19 cases in counties around SFO airport (b) No of people using SFO airport.

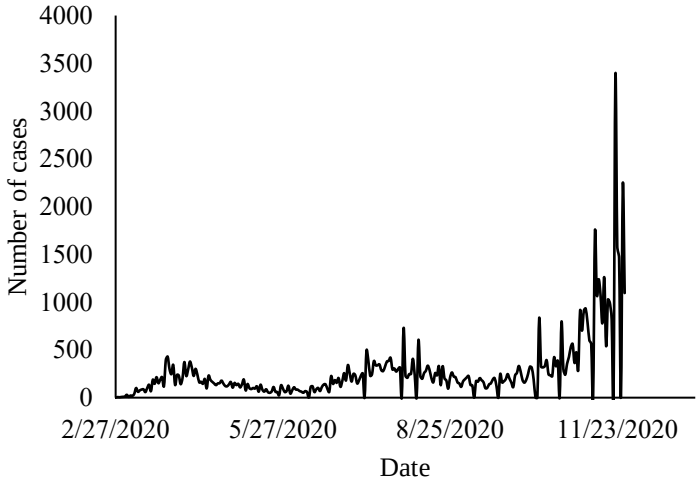

(a)

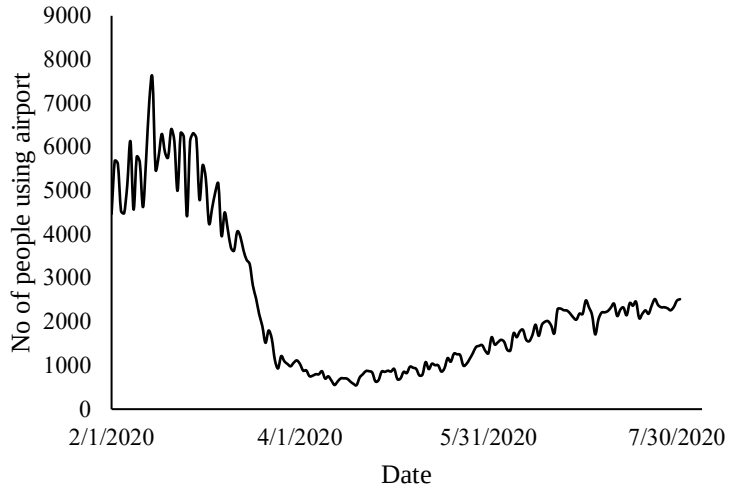

(b)

Figure 21 (a) Number of COVID-19 cases in counties around Seattle SEA airport (b) No of people using SEA airport.